STUDY OF MULTI-WALLED CARBON NANOTUBE EFFECT ON POLYVINYL ALCOHOL WITH CALCINED CUTTLEBONE

FOO TSI YIN

A project report submitted in partial fulfilment of the requirements for the award of Bachelor of Engineering (Honours.) Chemical Engineering

Lee Kong Chian Faculty of Engineering and Science
Universiti Tunku Abdul Rahman

April 2020

DECLARATION

I hereby declare that this project report is based on my original work except for citations and quotations which have been duly acknowledged. I also declare that it has not been previously and concurrently submitted for any other degree or award at UTAR or other institutions.

Signature : 

Name : Foo Tsi Yin

ID No. : 15UEB03332

Date : 12/5/2020

APPROVAL FOR SUBMISSION

I certify that this project report entitled **"STUDY OF MULTI-WALLED CARBON NANOTUBE EFFECT ON POLYVINYL ALCOHOL WITH CALCINED CUTTLEBONE"** was prepared by **FOO TSI YIN** has met the required standard for submission in partial fulfilment of the requirements for the award of Bachelor of Engineering (Honours.) Chemical Engineering at Universiti Tunku Abdul Rahman.

Approved by,

Signature : 

Supervisor : Ir Dr Lee Tin Sin

Date : 12/5/2020

ACKNOWLEDGEMENTS

I would like to thank everyone who had contributed to the successful completion of this project. I would like to express my gratitude to my research supervisor, Ir.Dr. Lee Tin Sin for his invaluable advice, guidance and his enormous patience throughout the development of the research.

In addition, I would also like to express my gratitude to my loving parents and friend (Mr Wong) who had helped and given me encouragement in order to complete this research.

ABSTRACT

The present study demonstrates the effects of multi-walled carbon nanotube (MWCNT) on polyvinyl alcohol (PVOH) with calcined cuttlebone. The aims of this study are to determine the mechanical, thermal and chemical properties as well as the morphology of MWCNT added with calcined cuttlebone in PVOH matrix. Since PVOH presents some drawbacks in bone scaffolding applications, MWCNT and calcined cuttlebone were used as reinforcing material in this study. Three compounds (PVOH-MWCNT-calcined cuttlebone) were blended together, cast and analysed. The loading of MWCNT incorporated was varied from 1 phr to 3 phr with 2 phr and 5 phr of calcined cuttlebone whereas the loading of PVOH was fixed at 100 phr. Characterization tests were made according to their mechanical properties, morphologies, interaction of bonding, crystallinity and thermal properties. Mechanical properties were observed to increase with increasing MWCNT loading in which the maximum tensile strength is 42.65 MPa for 2 phr calcined cuttlebone and 41.43 MPa for 5 phr calcined cuttlebone. Scanning electron microscopy (SEM) images suggested that agglomeration of MWCNT in PVOH matrix tends to occur at high loading (5phr) of calcined cuttlebone and well distribution was induced with increasing loading of MWCNT. X-ray diffraction (XRD) results showed that PVOH peaks were observed at the range of 19^{o}-21^{o} and crystallinity of PVOH/MWCNT composite is the highest at low (2phr) amount of calcined cuttlebone. Fourier transform infrared spectroscopy (FTIR) analysis showed that the interaction of bonding between molecules increased with increasing loading of MWCNT at low (2 phr) loading of calcined cuttlebone. Differential scanning calorimetry (DSC) results showed that the melting temperature increased with increasing loading of MWCNT at both 2 phr and 5 phr calcined cuttlebone. The highest enthalpy of melting is 44.46 J/g and 38.64 J/g at both 2 phr and 5 phr calcined cuttlebone respectively. In short, the mechanical and thermal properties increased with increasing loading of MWCNT but the matrix tends to agglomerate when minimum calcined cuttlebone content is exceeded whereas the addition of 2 phr calcined cuttlebone induced the strongest interaction of bonding between molecules.

TABLE OF CONTENTS

DECLARATION **i**
APPROVAL FOR SUBMISSION **ii**
ACKNOWLEDGEMENTS **iv**
ABSTRACT **v**
TABLE OF CONTENTS **vi**
LIST OF TABLES **ix**
LIST OF FIGURES **x**
LIST OF SYMBOLS / ABBREVIATIONS **xiii**

CHAPTER

1 INTRODUCTION **1**
1.1 Background of Research 1
1.2 Problem Statements 2
1.3 Aims and Objectives 3
1.4 Scope of the Study 3
1.4.1 Tensile Test 3
1.4.2 Scanning Electron Microscopy (SEM) 4
1.4.3 X-Ray Diffraction Analysis (XRD) 4
1.4.4 Fourier Transform Infrared Spectroscopy (FTIR) 4
1.4.5 Differential Scanning Calorimetry (DSC) 4

2 LITERATURE REVIEW **5**
2.1 Polyvinyl Alcohol (PVA) 5
2.2 Carbon Nanotube (CNT) As an Additives 6
2.2.1 Multi-Walled Carbon Nanotube (MWCNT) 7
2.2.2 Dispersion of MWCNT with Polymer Composites 8

		2.2.3 Functionalization of Multi-Walled Carbon Nanotube (MWCNTs)	8
	2.3	PVA/ CNT Composites	13
		2.3.1 Tensile Test	13
		2.3.2 Scanning Electron Microscopy (SEM) Test	15
		2.3.3 X-Ray Diffraction (XRD) Test	16
		2.3.4 Fourier Transform Infrared Spectroscopy (FTIR) Test	17
		2.3.5 Differential Scanning Calorimetry (DSC)	18
	2.4	Cuttlebone as an Addictive	20
		2.4.1 Calcination of Cuttlebone	21
		2.4.2 Hydroxyapatite (HAp)	23
		2.4.3 XRD Test on HAp	24
	2.5	Bone Scaffolding Reinforced by HAp	26
		2.5.1 Requirements for an Ideal Scaffold	26
		2.5.2 Advantages of Polymer Composite Scaffolds	27
	2.6	Polyvinyl Alcohol/ Hydroxyapatite (PVOH /HAp)	28
		2.6.1 Scanning Electron Microscopy (SEM)	29
		2.6.2 Fourier Transform Infrared Spectrometry (FTIR)	30
3	**METHODOLOGY**		**31**
	3.1	Materials	31
	3.2	Formulation	31
	3.3	Sample Preparation	32
	3.4	Testing	33
		3.4.1 Tensile Test	33
		3.4.2 Scanning Electron Microscope (SEM)	33
		3.4.3 X-ray Diffraction (XRD)	33
		3.4.4 Fourier Transform Infrared Spectroscopy (FTIR)	34
		3.4.5 Differential Scanning Calorimetry (DSC)	34

4	**RESULTS AND DISCUSSIONS**		**35**
	4.1	Tensile Strength	35
		4.1.1 Young's Modulus	37
		4.1.2 Elongation at Break	38
	4.2	Scanning Electron Microscopy (SEM)	40
	4.3	X-ray Diffraction (XRD)	44
		4.3.1 Crystallinity of Composite	44
		4.3.2 Crystallite Size of Composite	47
	4.4	Fourier Transform Infrared Spectroscopy (FTIR)	49
	4.5	Differential Scanning Calorimetry (DSC)	55
		4.5.1 Melting Temperature	55
		4.5.2 Enthalpy of Melting	58
5	**CONCLUSION AND RECOMMENDATIONS**		**60**
	5.1	Conclusion	60
	5.2	Recommendations	61
REFERENCES			**62**

LIST OF TABLES

TABLE	TITLE	PAGE
Table 2.1	Results of DSC Data for PVA with Different Loading of MWCNT	19
Table 2.2	Results of DSC Data for Reinforced PVA/MWCNTs Composite	20
Table 2.3	Chemical Composition of Cuttlebone	21
Table 2.4	Pore Size Distribution for Ideal Scaffold	27
Table 3.1	Composition of PVOH/MWCNT and Calcined Cuttlebone for Preparation of Sample	32
Table 4.1	Crystallite Size and d-Spacing at 2 phr Calcined Cuttlebone	48
Table 4.2	Crystallite Size and d-Spacing at 5 phr Calcined Cuttlebone	48

LIST OF FIGURES

FIGURE	TITLE	PAGE
Figure 2.1	Structural Formula for PVA: (a) partially hydrolysed and (b) fully hydrolysed	5
Figure 2.2	Stress against Strain for MWCNT	7
Figure 2.3	Photographs of Aggregation of MWCNT from SEM Test	8
Figure 2.4	Photomicrographs Illustrating Poor Dispersion	9
Figure 2.5	Photomicrographs Illustrating Good Dispersion	9
Figure 2.6	Functionalization Process	10
Figure 2.7	FTIR Spectra of CNT-H, CNT-Ac and CNT-DDA	11
Figure 2.8	Tensile Strength of MWCNT/ Polymer Composite	12
Figure 2.9	Young's Modulus of MWCNT/ Polymer Composite	12
Figure 2.10	Tensile Strength of PVA/MWCNT Composite with Different MWCNT Concentration (%)	14
Figure 2.11	Elongation Break of PVA/MWCNT Composite with Different MWCNT Concentration (%)	14
Figure 2.12	Morphologies of PVA/MWCNT at (a): MWCNT-0, (b) MWCNT-2, (c) MWCNT-5, (d) MWCNT-10	15
Figure 2.13	XRD of (a) pure PVA, (b) 0.3 SWCNTs/PVA, (c) 0.7 SWCNTs/PVA, (d) 0.3 MWCNTs/PVA and (e) 0.7 MWCNTs/PVA	16

Figure 2.14	FTIR Spectra of PVA/MWCNT Composites at: (a) 0%, (b) 10%, (c) 20%, (d) 30%, (e) 40% (v/v)	17
Figure 2.15	DSC Curve of PVA Nanofibers with Different Loading of MWCNTs	18
Figure 2.16	(A) Digital Photograph of a Dorsal-View Cuttlebone Cut through the Cross-Section, (B) Schematic Transverse Section through the Cuttlebone, (C) Digital Photograph of A Block Cut from Lamellar Part of the Bone, (D) SEM of the Bone	21
Figure 2.17	Percentage of Apatite Mineral Phase, Amorphous (Grey) and Crystalline (White)	22
Figure 2.18	FTIR Spectrum of Cuttlebone at Different Calcination Temperature	23
Figure 2.19	XRD Pattern of (a) Bone Ash at Different Temperature; (b) 600 ℃, (c) 700 ℃, (d) 800 ℃ and (e) 1100 ℃	25
Figure 2.20	Bone Scaffold	26
Figure 2.21	SEM Image of HA/PVOH Composite with Various HA Content	29
Figure 2.22	FTIR Spectra of Pure PVOH and PVOH/HA Composites	30
Figure 4.1	Tensile Strength of PVA/MWCNT Composite with Different Loading of Calcined Cuttlebone and MWCNT	37
Figure 4.2	Young's Modulus of PVA/MWCNT Composite with Different Loading of Calcined Cuttlebone and MWCNT	38
Figure 4.3	Elongation of Break of PVA/MWCNT Composite with Different Loading of Cuttlebone and MWCNT	39

Figure 4.4	Surface Morphology of PVOH/MWCNT Composite at 2 phr of Calcined Cuttlebone added with Different Loading of MWCNT (a) 1 phr MWCNT (b) 2 phr MWCNT (c) 3 phr MWCNT	42
Figure 4.5	Surface Morphology of PVOH/MWCNT Composite at 5 phr of Calcined Cuttlebone added with Different Loading of MWCNT (a) 1 phr MWCNT (b) 2 phr MWCNT (c) 3 phr MWCNT	43
Figure 4.6	XRD Pattern of PVA with Different Loading of MWCNT at 2 phr Calcined Cuttlebone	45
Figure 4.7	XRD Pattern of PVA with Different Loading of MWCNT at 5 phr Calcined Cuttlebone	46
Figure 4.8	Crystallinity of PVA with Different Loading of MWCNT and Calcined Cuttlebone	47
Figure 4.9	FTIR Spectra of PVOH with Different Loading of MWCNT at 2 phr Calcined Cuttlebone	52
Figure 4.10	FTIR Spectra of PVOH with Different Loading of MWCNT at 5 phr Calcined Cuttlebone	53
Figure 4.11	Hydroxyl Group of PVOH with Different Loading of MWCNT and Calcined Cuttlebone	54
Figure 4.12	C-H Bonds of PVOH with Different Loading of MWCNT and Calcined Cuttlebone	54
Figure 4.13	DSC Result for PVOH with Different Loading of MWCNT at 2 phr Calcined Cuttlebone	56
Figure 4.14	DSC Result for PVOH with Different Loading of MWCNT at 5 phr Calcined Cuttlebone	57
Figure 4.15	Melting Temperature for PVOH with Different Loading of MWCNT and Calcined Cuttlebone	57
Figure 4.16	Enthalpy of Melting for PVOH with Different Loading of MWCNT and Calcined Cuttlebone	59

LIST OF SYMBOLS / ABBREVIATIONS

Ca	Calcium
Ca/P	Calcium to Phosphate Ratio
$CaCO_3$	Calcium Carbonate
CaO	Calcium Oxide
CNT	Carbon Nanotube
CNT-Ac	Carbon Nanotube after Vacuum
CNT-H	Pristine Carbon Nanotube
DDA	Dodecylamine
DSC	Differential Scanning Calorimetry
FTIR	Fourier Transform Infrared Spectroscopy
HAp/HA	Hydroxyapatite
Mg^{2+}	Magnesium Ion
MWCNTs	Multi-Walled Carbon Nanotubes
Na^{+}	Sodium Ion
OH	Hydroxyl
P	Phosphorus
PVA/CNT	Polyvinyl Alcohol/Carbon Nanotube
PVA/MWCNT	Polyvinyl Alcohol/ Multi-Wall Carbon Nanotube
PVA/PVOH	Polyvinyl Alcohol
SEM	Scanning Electron Microscope
SWCNTs	Single-Walled Carbon Nanotubes
TGA	Thermogravimetric Analysis
XRD	X-Ray Diffraction
Zn^{2+}	Zinc Ion

ΔC_p	Specific Heat Values, J/g ℃
ΔH	Enthalpy of Melting, J/g
T_g	Glass Transition Temperature, ℃
T_m	Melting Temperature, ℃
X	Crystallinity, %

CHAPTER 1

INTRODUCTION

1.1 Background of Research

In recent studies, natural polymers were limited in the ability to obtain extensive commercial application due to their weakness in mechanical properties. Significant improvement of the properties such as toughness, strength and stiffness can be accomplished through the incorporation of various kinds of organic and inorganic fillers. Inorganic fillers were substituted by natural composites due to environmental issues. In order to attain high mechanical characteristics at reduced filler loading, natural composites such as cuttlebone and nanofiller which is multi-walled carbon nanotube (MWCNT) were used as reinforcing materials for polyvinyl alcohol (PVA) in this research study.

Composite material consists of two or more materials and works together to give unique properties. Natural composites can be obtained from animal bones. Composite synthesized from collagen and hydroxyapatite are known as candidate of scaffold due to their composition is analogous to the extracellular matrix of natural bone (Tontowi, et al., 2016). Cuttlebone is considered as natural composite material which can be found naturally and it is better than artificial composite.

Hydroxyapatite (HAp) is a bioceramic which is widely used for bone tissue repair due to its biocompatibility, exceptional mechanical strength and osteoconductivity (Venkatesan, et al., 2018). HAp can be obtained through synthetic and natural ways. The natural method to obtain HAp is thermal calcination to extract and isolate HAp from animal bones (Venkatesan, et al., 2018). In this research, cuttlebone was treated under thermal calcination to obtain hydroxyapatite powder.

Significant studies have been made in the field of reinforcement of polymer compounds with composite material as well as nanofiller. One of the methods to improve the compressive strength of HAp and bone composite is by blending with synthetic polymer (Tontowi, et al., 2016). Among these synthetic polymers, PVA has received most of the attention due to its physiochemical properties and biocompatible with better thermal stability, tensile strength as

well as flexibility (Kaur and Thirugnanam, 2016). However, the weak mechanical properties of PVA often leads to failure in some engineering applications. Hence, the mechanical properties of PVA could be improved with biocompatible reinforcement in PVA matrix. (Kaur and Thirugnanam, 2016). Involvement of carbon-based biomaterials in polymer matrix contributes to high mechanical and biological properties (Kaur and Thirugnanam, 2016).

MWCNT has received most of the attention from researchers due to their remarkable mechanical and electrical properties and act as the most promising nanofiller for polymer composite (Choudhary and Gupta, 2011). The excellent properties of MWCNT can be exploited if they are homogeneously embedded into other materials in the form of composites or light-weight matrices (Spitalsky, et al.,2010). MWCNT/polymer composites with high strength properties can be achieved only in the case of well interaction of MWCNT within the matrix (Li, J.,2017).

There are two basic types of CNT which are single-wall carbon nanotubes (SWCNTs) and multi-wall carbon nanotubes (MWCNTs). MWCNT were used in this research due to better enhancement in mechanical, thermal and electrical properties. MWCNTs consist of multiple concentric layers of graphene composing it, therefore it is stronger than SWCNTs. The open end of MWCNTs has a fast electron rate which contributes to better electrical properties. Besides, MWCNTs is cheaper in production as material modification.

1.2 Problem Statements

Over the past few years, attentions have been given to the development of reinforced polymer composite. Among other carbon compounds, MWCNT will be the most suitable choice to blend in with polymer composite. Animal bone which act as a natural composite possess the capability to further improve the mechanical properties of polymer composite.

MWCNT has gained much attention because they offer excellent physical, chemical and biological properties which is compatible in many engineering fields. Besides, unique functionalization improves the interaction between polymer and MWCNT. This research study was tested on the characterization

of PVA with calcined cuttlebone and MWCNT. The change of sample properties was tested with different amount of MWCNT and calcined cuttlebone.

The problem statements are:

i. What are the effects of MWCNT in terms of mechanical properties and morphology on PVA with calcined cuttlebone?

ii. What are the effects of MWCNT in terms of thermal and chemical properties on PVA with calcined cuttlebone?

1.3 Aims and Objectives

The aims and objectives were to study the properties of PVA/MWCNT composite after adding calcined cuttlebone. The study included bonding interaction, morphology of composite, mechanical, chemical and thermal properties. List of objectives were:

i. To determine the effects of MWCNT in terms of mechanical properties and morphology on PVA with calcined cuttlebone.

ii. To determine the effects of MWCNT in terms of thermal and chemical properties on PVA with calcined cuttlebone.

1.4 Scope of the Study

Based on the aims and objectives, the characterization of PVA-MWCNT with calcined cuttlebone were studied through several characterization techniques.

1.4.1 Tensile Test

Tensile test was used to determine the mechanical properties of the composites. Besides, the force required to break the blended specimen was examined and how the specimen react on stress and strain in elongation or stretching to its breaking point was observed. Furthermore, tensile strength, elongation percentage and Young's modulus for the composites were tested using tensile test. The composites were subjected to an amount of stress and strain until the specimen break into two single parts.

1.4.2 Scanning Electron Microscopy (SEM)

In this research study, SEM was used to study topography and morphology. This technique was used to determine the overall morphology of PVA/MWCNT/cuttlebone composite. It was simple to operate and user-friendly However, sample preparation was required before performing SEM analysis and the sample must be in solid form.

1.4.3 X-Ray Diffraction Analysis (XRD)

In this research, XRD was used to identify the crystalline phases for PVA/MWCNT/cuttlebone composite. The properties of materials such as hardness, density and transparency are mainly dependant on the crystal structure. Each component has a characteristic pattern of diffraction and respective intensity of diffracted beam. The degree of crystallinity of the composite were determined through XRD test.

1.4.4 Fourier Transform Infrared Spectroscopy (FTIR)

FTIR is an analytical technique to examine the interaction of bonding between two composites and it is used as a quantitative tool to identify the specific functional groups present in a sample. In this research study, FTIR was used to identify the chemical features that occur due to addition of calcined cuttlebone and MWCNT at different component ratio. The result was obtained via FTIR spectrograph.

1.4.5 Differential Scanning Calorimetry (DSC)

Differential Scanning Calorimetry (DSC) in this research study was used to measure the melting temperature and enthalpy of melting associated with thermal transitions in the polymer composites.

CHAPTER 2

LITERATURE REVIEW

2.1 Polyvinyl Alcohol (PVA)

Polyvinyl Alcohol (PVA) has exceptional optical properties, large dielectric strength and outstanding ability for charge storage. Doping with nanofillers can easily customize its mechanical, optical and electrical properties. (Aslam, Kalyar and Raza, 2018).

Unlike most polymers, PVA does not undergo polymerization of the corresponding monomer due to its unstable nature. It is essentially produced from polyvinyl acetate through partial or complete hydrolysis to remove acetate group in an environment of aqueous sodium hydroxide. PVA is a biodegradable polymer and due to the presence of hydroxyl groups on the carbon atoms, its degradability can be enhanced through hydrolysis (Gaaz, et al., 2015). The amount of hydroxyl groups present in polymer determines the physiochemical and mechanical properties of PVA. Figure 2.1 shows the structural formula for PVA as (a) partially hydrolysed and (b) fully hydrolysed.

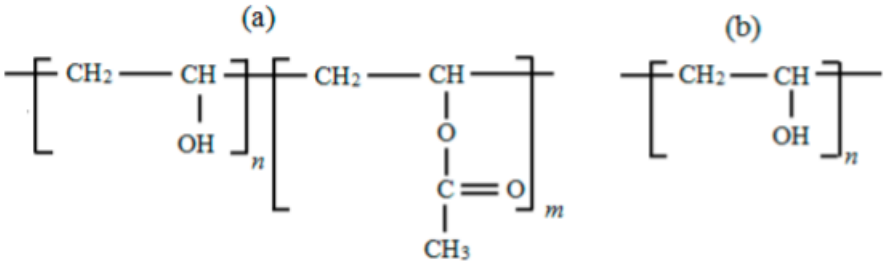

Figure 2.1: Structural Formula for PVA: (a) Partially Hydrolysed and (b) Fully Hydrolysed (Gaaz, et al., 2015)

Fully hydrolysed PVA has different properties compared to partially hydrolysed PVA due to the amount of hydroxyl groups present within the compound. The properties of a fully hydrolysed PVA can be altered through crosslinking of linear polymers (Gaaz, et al., 2015). Polymer contents affect the physical state of PVA. A higher polymer content results in high stiffness and high strength for a material's matrix.

Fully hydrolysed PVA is having a higher degree of hydrolysis, which is 98 % - 99 % while partially hydrolysed PVA is having 84.2 % -89 % degree of hydrolysis. Fully hydrolysed is more preferable due to its greater stiffness and strength.

The physical properties of PVA depends on the degree of hydrolysis, crystal precipitation, molecular mass and moisture (Aslam, Kalyar and Raza, 2018). PVA with different properties such as structural, optical, mechanical and electrical properties can be altered by blending a small amount of nanofillers (Aslam, Kalyar and Raza, 2018). Nanofillers expose its large surface area for PVA to interact with it which leads to enhancement of functional properties (Aslam, Kalyar and Raza, 2018). PVA is often investigated due to its compatible structure, hydrophilic properties and various use in cross-linked products. Macromolecules can form crystallites by annealing amorphous PVA films above 85℃, stabilizing the films and inducing a chemically cross-linked behaviour.

2.2 Carbon Nanotube (CNT) As an Additives

Small amount of nanofillers which is lesser than 5 wt % are most widely used to enhance the properties of polymers due to their high aspect ratio. Nanofillers possess large surface area for interaction with surrounding matrix which lead to excellent properties of polymer composite. Besides, nanofillers has a quantum confinement effect which makes the interaction of CNT/polymer composites superior.

The nanoparticles dispersion state is the leading challenge in obtaining the complete potential of properties enhancement. In order to achieve large interfacial area between the constituents of nanocomposites, uniform dispersion must be accomplished. There are several impacts attributed by the reinforcing effect of filler such as properties of polymer matrix, nature and type of nanofiller, aspect ratio and particle distribution. The evaluation of nanofiller dispersion is related to the morphologies obtained (Oliveira and Beatrice, 2018).

The incorporation of CNT in polymer matrices is used to obtain composite materials with superior mechanical strength and thermal properties. CNT has a break strength as high as 200 GPa and the elastic moduli in 1 TPa range. Besides, the approximately 500 times increase in surface area per gram and aspect ratios of around 10^3 has prompted a huge interest in using CNTs as reinforcing phase for polymer matrices.

2.2.1 Multi-Walled Carbon Nanotube (MWCNT)

CNTs are categorised into two types which are single-wall carbon nanotube (SWCNT) and multi-wall carbon nanotube (MWCNT). MWCNT is composed of multiple layers of graphene while SWCNT is composed of single layer of graphene. According to Choudhary and Gupta (2011), several of experimental studies have been examined to determine the mechanical MWCNT. Figure 2.2 shows the graph of stress (GPa) against strain (%).

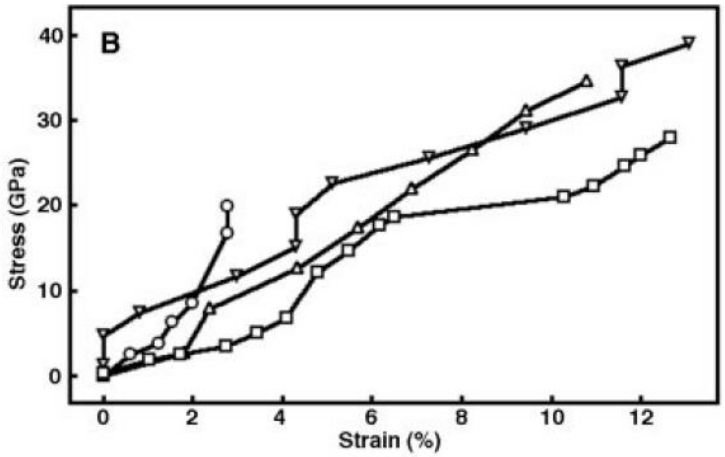

Figure 2.2: Stress against Strain for MWCNT (Yu, et al., 2000)

According to the result obtained from TEM and in-situ tensile test, the stiffness values are 1.8 TPa for MWCNT and 1.25 TPa for SWCNT (Yu, et al., 2000). In addition, the strength ranged from 11 to 63 GPa is observed at the outer shell of MWCNT with maximum fracture strains up to 12% and modulus value ranged from 270 to 950 GPa. For SWCNT, the strain value is 5.3% or lower. The number of defects and interlayer interactions in MWCNTs effects the strength of CNTs (Choudhary and Gupta, 2011).

2.2.2 Dispersion of MWCNT with Polymer Composites

According to Andrews and Weisenberger (2003), a loading of 1 wt % MWCNTs was randomly distributed in an ultra-high molecular weight polyethylene film, the strain energy density has increased by 150 % and the ductility has increased by 140 %.

Another similar effect was found in MWCNT/polyacrylonitrile fibers which contained 1.8 % of MWCNTs. The composite has 80 % increase in energy yield. Besides, an addition of 1 wt % MWCNTs to isotactic polypropylene increase the crystallization rate for the composite material.

One of the factors that affect the composite's modulus is MWCNT distribution. As the concentration of MWCNT increase, the diameter of composite nanofibers will decrease.

According to Sankar, Reddy and Prasad (2015), thermal stability test was performed with TGA for polydimethylsiloxane/MWCNT, the specimen with 4.28 % MWCNT has thermal stability of 273 ℃. When the specimen is mixed with 6 wt % MWCNT, the thermal stability has increased to 322 ℃.

2.2.3 Functionalization of Multi-Walled Carbon Nanotube (MWCNTs)

A great dispersion of filler with the matrix is very important to prevent aggregation of the filler. MWCNTs form aggregates easily during compounding due to large surface area. Occurrence of aggregation is due to Van der Waal force taken place between nanocarbon particles (Wongon, Thumsorn and Srisawat, 2016). Figure 2.3 shows the photographs of Aggregation of MWCNT from SEM test.

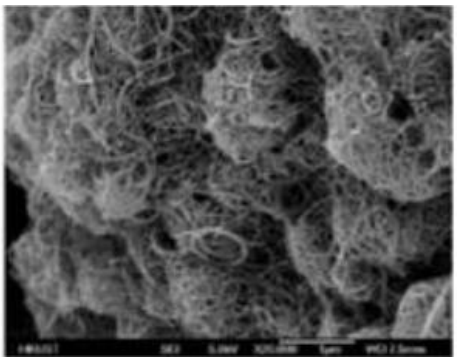

Figure 2.3: Photographs of Aggregation of MWCNT from SEM Test (Wongon, Thumsorn and Srisawat, 2016)

The aggregation shapes are agglomerate style for MWCNTs. In order to achieve well dispersion and to prevent aggregation, MWCNTs can be chemically modified to improve the interfacial interaction (Oliveira and Beatrice, 2018). Figure 2.4 shows the photomicrographs illustrating poor dispersion while Figure 2.5 shows photomicrographs illustrating good dispersion.

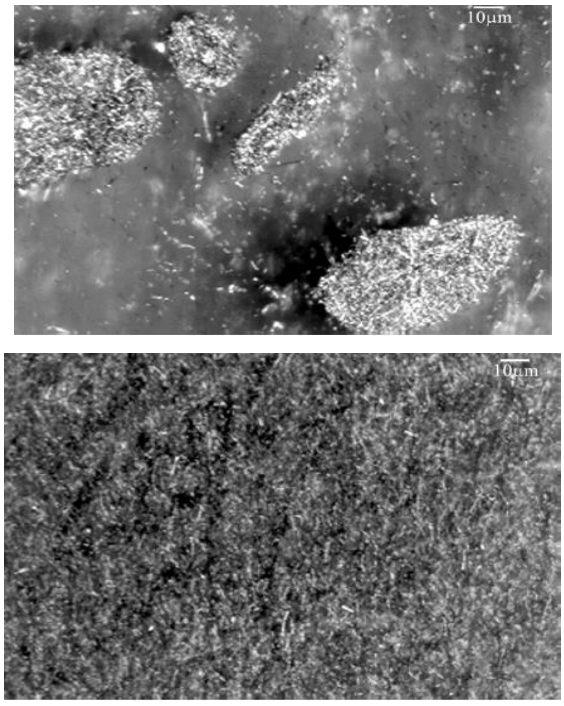

Figure 2.4: Photomicrographs Illustrating Poor Dispersion (Andrews, et al., 2002)

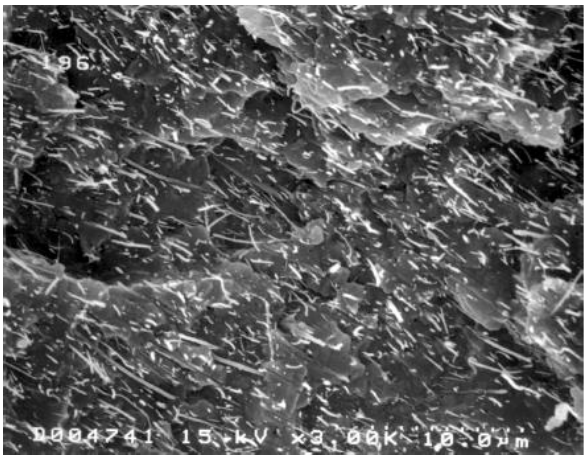

Figure 2.5: Photomicrographs Illustrating Good Dispersion (Andrews, et al., 2002)

As seen from Figure 2.4, the dispersion of MWCNT is poor in the matrix due to the presence of many clumps and agglomerates. Besides, inside the mixing zone where the presence of different concentrations of dispersed nanofibers as well as the existence of discontinuities at the boundaries has proven the poor mixing in the matrix (Andrews, et al., 2002) whereas in Figure 2.5, a uniform fiber density distribution without agglomeration can be observed from the SEM image.

The effective way to stabilize dispersion and avoid agglomeration of CNTs is to perform surface functionalization of CNTs (Choudhary and Gupta, 2011).

According to Ferreira, et al. (2017), functionalization with nonpolar molecule which is dodecylamine (DDA) produces alkyl group on the surface of CNTs. This could prevent agglomeration due to “steric factors” and promote well interactions between the molecule. Other researcher found that when surface functionalization is done on the surface of CNTs, the dispersion in the solvent will improve due to the strong interaction of the functional group attached to the CNTs and polymer matrix (Morelli, et al., 2015). Figure 2.6 shows the functionalization process to determine the functional group of different matrices.

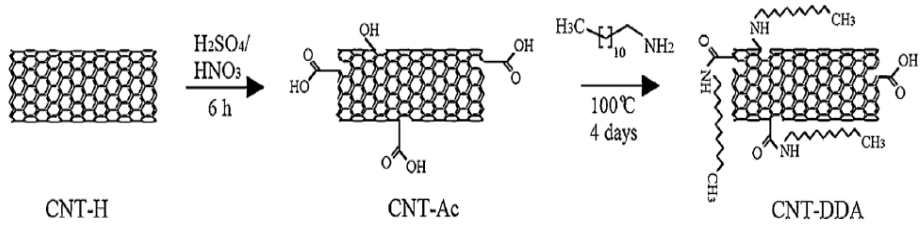

Figure 2.6: Functionalization Process (Ferreira, et al., 2017)

Pristine carbon nanotube (CNT-H) will be treated with concentrated sulfuric acid or nitric acid and the product will be labelled as CNT-Ac. CNT-Ac will be mixed with DDA to form CNT-DDA.

The changes on the surface of CNTs produced by the functional groups was observed using FTIR. Figure 2.7 shows the FTIR spectra of CNT-H, CNT-Ac and CNT-DDA.

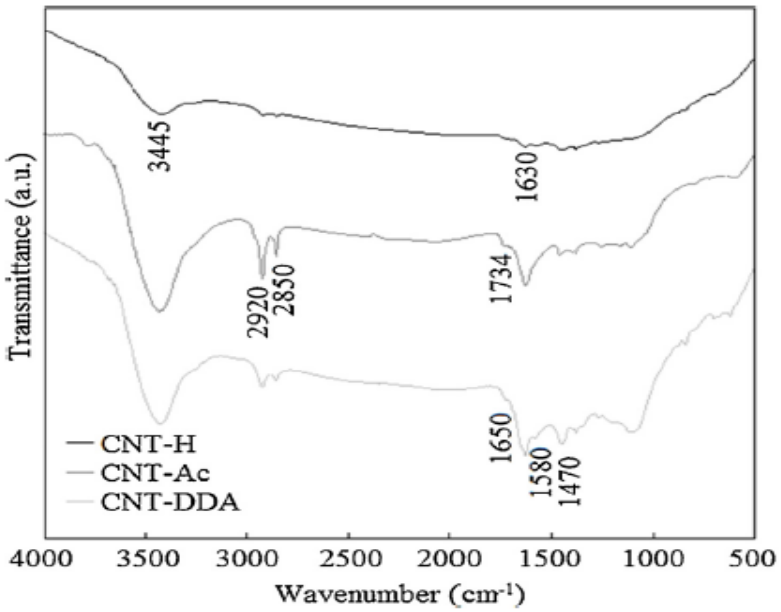

Figure 2.7: FTIR Spectra of CNT-H, CNT-Ac and CNT-DDA (Ferreira, et al., 2017)

FTIR spectrum of CNT-Ac has showed the presence of carbonyl stretch of the carboxylic acid group (Ferreira, et al., 2017). The intensity of double bond has increased due to the presence of carboxylated CNTs (Ferreira, et al., 2017).

Surface treatment with mixture of nitric and sulphuric acid which resulted in the formation of carboxylic acid on the surface is one of the routes to modify CNTs. Besides, secondary particles such as clay can be used to improve the dispersion of CNTs in polymer matrix. In addition, polymer blends as matrix have been used to improve the thermal properties of the composites (Andrews, et al., 2002).

Polymer nanocomposite is fabricated by in situ polymerization, solution or melt blending. In order to produce MWCNT/polymer through a more practical way, shear mixing can be carried out (Andrews, et al., 2002). According to Andrew, et al. (2002), the physical properties of polymers are also determined by molecular size and distribution. Figure 2.8 shows the tensile strength of MWCNT/ polymer composite while Figure 2.9 shows the Young's modulus of MWCNT/ polymer composite.

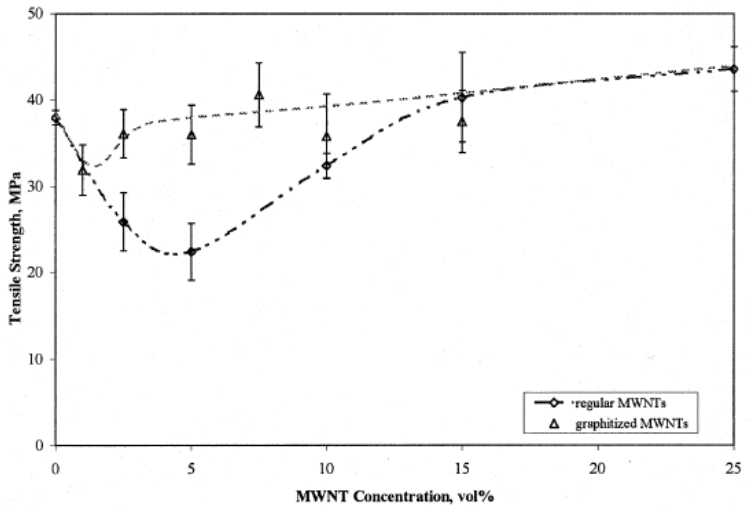

Figure 2.8: Tensile Strength of MWCNT/ Polymer Composite (Andrews, et al., 2002)

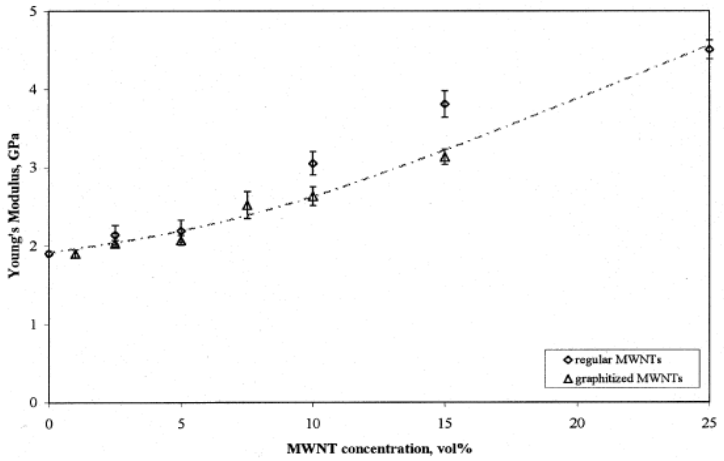

Figure 2.9: Young's Modulus of MWCNT/ Polymer Composite (Andrews, et al., 2002)

As seen from Figure 2.8, composites which contain 2.5 vol % - 25 vol % of MWCNTs, Young's modulus increased tremendously from 1.9 GPa to 4.5 GPa. However, in Figure 2.9, the tensile strength has reduced at low MWCNT concentrations which are 0.05 vol % to 0.5 vol %. As the concentration of MWCNT increased, the Young's modulus of the composite increased as well.

2.3 PVA/ CNT Composites

Incorporation of CNT in PVA contributes to significant improvement in mechanical, thermal and electrical properties of polymer composites. There are several factors that influence the properties modification which includes type of CNT, aspect ratio of CNT ratio and processing method. In order to obtain the desired properties, the conditions have to be optimized with appropriate amount of CNTs into the polymer. A small fraction of CNTs incorporated in PVA can lead to high modulus and high strength of a polymer matrix. Besides, good interfacial bonding between the nanofillers and polymer matrix is highly dependent on the interfacial bonding. Hence, load transfer between the composites will be influenced by interfacial shear stress between the components (Choudhary and Gupta, 2011). High interfacial shear stress will transfer the load in a short distance while low interfacial shear stress will transfer the load in longer period. (Choudhary and Gupta, 2011). Besides, incorporation of CNT into PVA will stabilize the thermal stability and increase the melting temperature. Polymer composite has been used as material in many engineering applications such as component due to their high durability, corrosion resistance, excellent electrical properties, high strength and light density. The most widely used of CNT nanocomposites are used in electronics, space exploration, high-end sporting goods and housing structures.

2.3.1 Tensile Test

According to Cadek, et al. (2002), an addition of 1 wt % of MWCNTs in PVA matrix was able to enhance the Young's modulus and hardness by 1.8 times and 1.6 times respectively. Dispersion of MWCNT in PVA enhanced the mechanical and thermal properties of the polymer matrix. According to Maghfirah, et al. (2018), they have conducted an experiment to test out the tensile strength and elongation at break for PVA/MWCNT composite. Figure 2.10 shows the tensile strength of PVA/MWCNT composite with different amount of MWCNTs while Figure 2.11 shows the elongation break of PVA/MWCNT composite with different amount of MWCNTs.

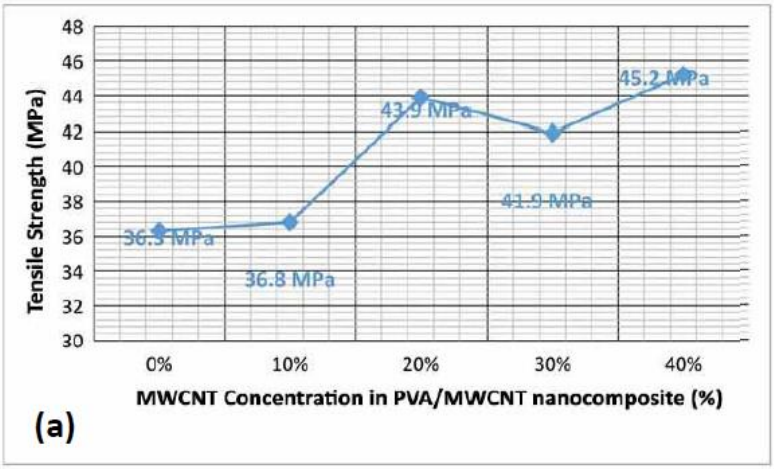

Figure 2.10: Tensile Strength of PVA/MWCNT Composite with Different MWCNT Concentration (%) (Maghfirah, et al., 2018)

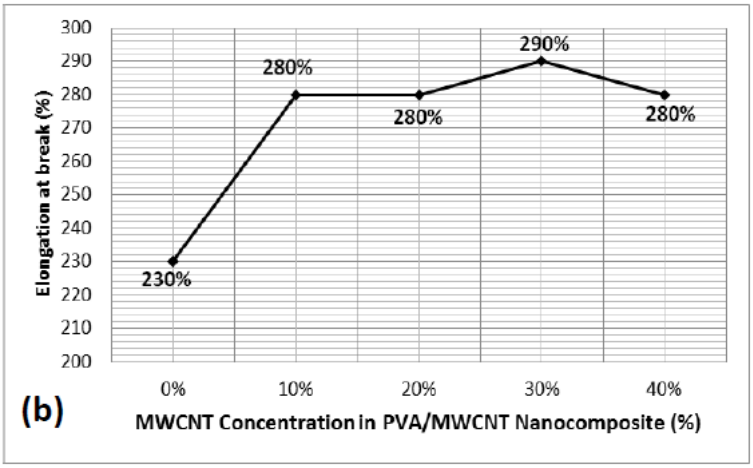

Figure 2.11: Elongation Break of PVA/MWCNT Composite with Different MWCNT Concentration (%) (Maghfirah, et al., 2018)

The tensile strength increased with higher amount of MWCNT in which the maximum tensile strength of the composite can reach 45.2 MPa while the minimum tensile strength is 36.5 MPa. This is due to MWCNTs have increased the restriction of "chain mobility" of PVA (Yee, et al, 2018). Besides, another possible reason is the complete "infiltration" of PVA into MWCNTs network (Yee, et al, 2018).

Well mixing of PVA solution into porous MWCNTs network has improved the interfacial bonding between PVA/MWCNTs composite and thus increased the mechanical strength.

As seen in Figure 2.11, the elongation at break increased from 230% to 280% with 10% of MWCNTs concentration in PVA/MWCNT composite. It reached the highest point at 290% and decreased to 280% at 40% of MWCNTs concentration in PVA/MWCNT composite. This was possibly due to an "embrittlement" of nanocomposite or due to the presence of agglomeration (Jogi, et al, 2012).

2.3.2 Scanning Electron Microscopy (SEM) Test

According to Wongon, Thumsorn and Srisawat (2016), they have conducted experiment on PVA/MWCNT composite by electrospinning techniques at four different formulas to determine the morphology of the composites. Figure 2.12 shows the morphologies of PVA/MWCNT at four different formulas.

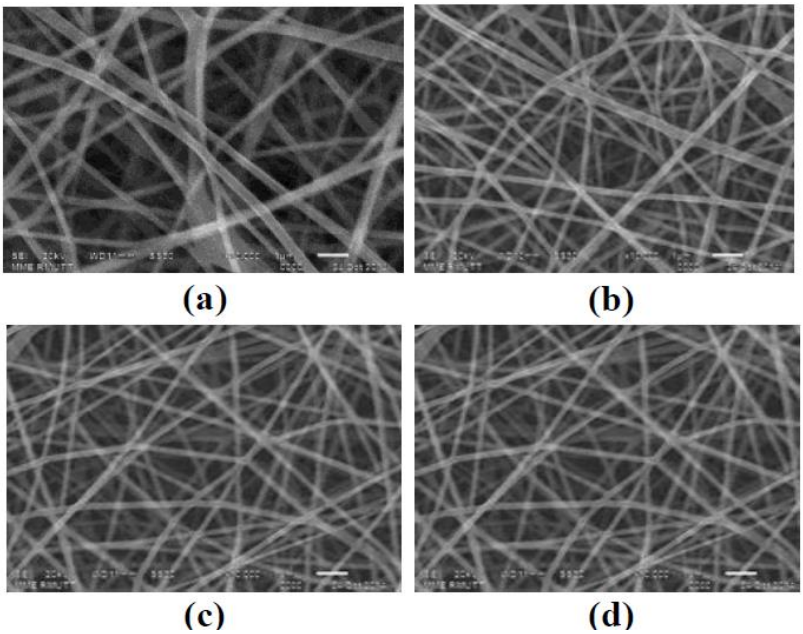

Figure 2.12: Morphologies of PVA/MWCNT at (a): MWCNT-0, (b) MWCNT-2, (c) MWCNT-5, (d) MWCNT-10 (Wongon, Thumsorn and Srisawat, 2016)

At MWCNT-0, the surface of nanocomposite is smooth and no “beads” are present in the composite nanofibers. At MWCNT-2, more “beads” are present and it is smaller compared to MWCNT-0. At MWCNT-5, more “beads” are present and the composite nanotube is even smaller compared to MWCNT-0 and MWCNT-2. At MWCNT-10, the surface is rough and many “beads” are present.

2.3.3 X-Ray Diffraction (XRD) Test

According to Diouri and Baitoul (2013), the experiment was conducted on two types of CNTs with different formulas to determine the crystallinity of the composites. Figure 2.13 shows the XRD of (a) pure PVA, (b) 0.3 SWCNTs/PVA, (c) 0.7 SWCNTs/PVA, (d) 0.3 MWCNTs/PVA and (e) 0.7 MWCNTs/PVA.

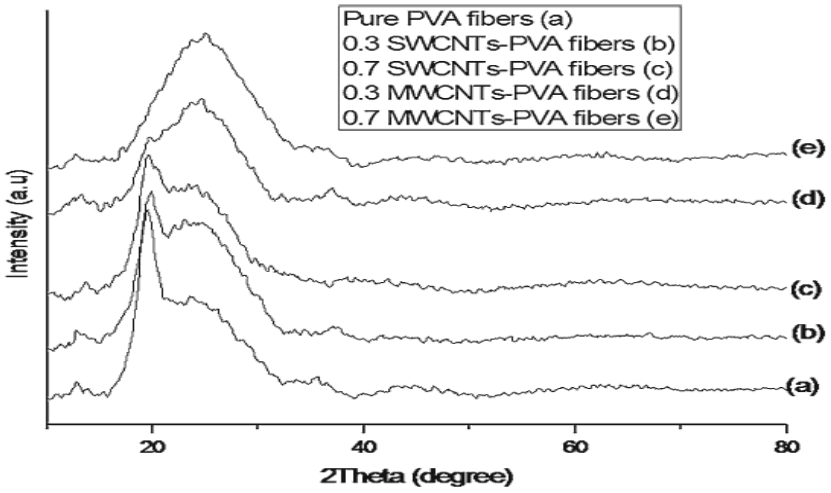

Figure 2.13: XRD of (a) pure PVA, (b) 0.3 SWCNTs/PVA, (c) 0.7 SWCNTs/PVA, (d) 0.3 MWCNTs/PVA and (e) 0.7 MWCNTs/PVA (Diouri and Baitoul, 2013)

As seen in Figure 2.13, pure PVA shows diffraction peaks at 2θ= 19.5° and 24.1° at (101) and (200) planes of "semi-crystalline" PVA (Diouri and Baitoul, 2013). The diffraction occurred due to "intermolecular interference" in the direction of "intermolecular" hydrogen bonding between PVA polymer chains. As the intensity of diffraction increased, the number of PVA chains packing increased as well.

For SWCNTs, as the concentration increased, the diffraction peak of pure PVA became lower and broader. The broader the diffraction peak, the lower the crystallinity of the composites. PVA (Diouri and Baitoul, 2013).
This is due to the "hydrogen-bonding" interaction between SWCNTs/PVA composite.

For MWCNTs, the peak of PVA has shifted higher when the concentration of MWCNTs increase from 0.3 to 0.7. This is due to strong interaction between MWCNTs and PVA molecules.

2.3.4 Fourier Transform Infrared Spectroscopy (FTIR) Test

According to Maghfirah, et al. (2018), they have conducted an experiment to test the changes of functional group for PVA/MWCNT composite using FTIR test. Figure 2.14 shows the FTIR Spectra of MWCNT/PVA composites.

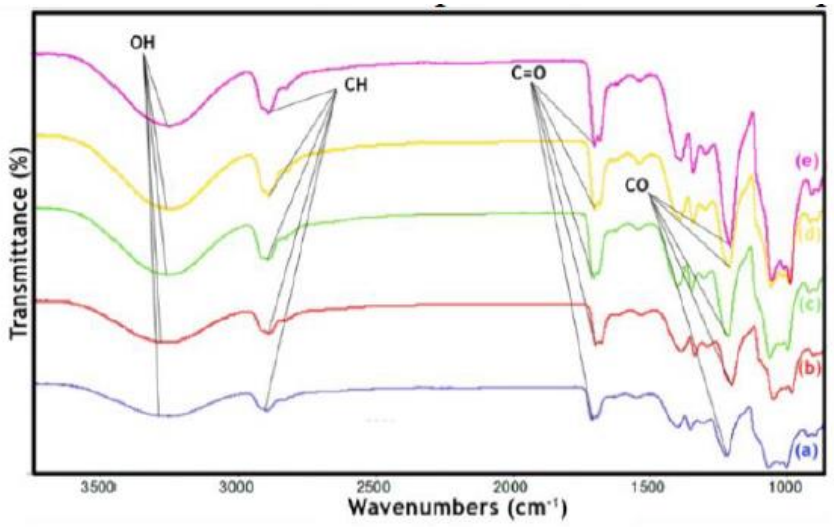

Figure 2.14: FTIR Spectra of PVA/MWCNT Composites at: (a) 0%, (b) 10%, (c) 20%, (d) 30%, (e) 40% (v/v) (Maghfirah, et al., 2018)

There is a peak around 3200 cm^{-1} which indicates the present of hydroxyl groups of MWCNT. The peak around 1700 cm^{-1} represents carbonyl group while the peak around 1500 cm^{-1} shows carboxylic group. From 0% to 40%, the presence of hydroxyl group can be represented by the broad peak around 3270 cm^{-1}, 3280 cm^{-1}, 3279 cm^{-1} and 3275 cm^{-1}.

Better interactions between the hydroxyl groups of PVOH and the carboxyl groups of MWCNT was due to the presence of hydrogen bonding between "hydrophilic" oxygen-containing functional groups (Yee, et al, 2018). PVA solution contains hydroxyl group (-OH) while MWCNT contain a few functional groups which will interact with the hydroxyl group of PVA. They are hydroxyl group (-OH), carbonyl group (C=O) ad carboxyl group (-COOH) on the surface of MWCNTs. The dispersion of MWCNT in PVA causes the strong "interfacial adhesion" between functionalized MWCNTs and PVA matrix.

2.3.5 Differential Scanning Calorimetry (DSC)

The experiment was carried out by Ekrem (2017) to test the glass transition temperature (T_g), specific heat values (ΔC_p), thermal stability and melting temperature (T_m) of polyvinyl alcohol reinforced with different weight ratios of multi-walled carbon nanotube by electro-spinning method. The result of reinforced PVA with 1%,3% and 5% of MWCNT is shown in Figure 2.15.

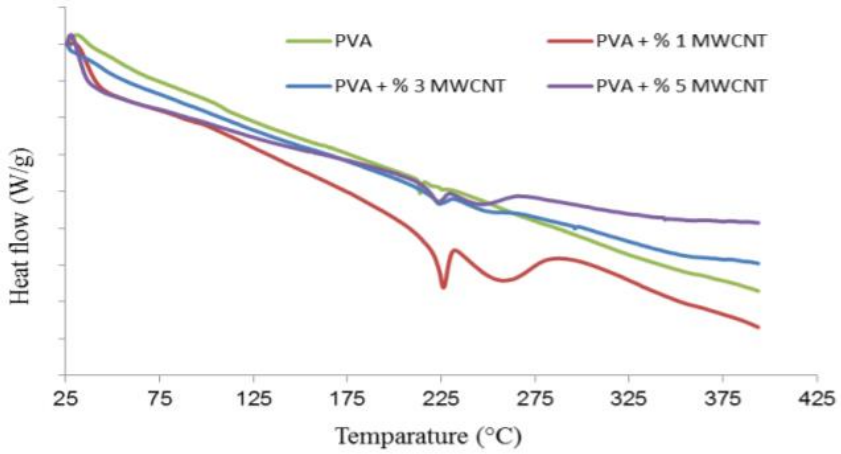

Figure 2.15: DSC Curve of PVA Nanofibers with Different Loading of MWCNTs (Ekrem, 2017)

PVA matrix shows no reaction before the melting temperature. According to DSC curve, no crystallization is formed during DSC heating study (Ekrem, 2017). The temperature has increased from 215 ℃ to 225 ℃ when 1% of MWCNT is added in PVOH as compared to pure PVOH. However, the glass transition temperature decreased when the concentration of MWCNT reached 5%. One of the reasons that causes the reduction is due to agglomeration in PVA matrix with higher amount of MWCNT. Table 2.1 shows the results for glass transition temperature, thermal stability, melting temperature and specific heat values of PVA reinforced with different loading of MWCNTs.

Table 2.1: Results of DSC Data for PVA with Different Loading of MWCNT (Ekrem, 2017)

Nanofiber Composites	**T_g(℃)**	**ΔC_p (J/g ℃)**	**Thermal Stability (℃)**	**T_m(℃)**
PVA	77	0.066	205	215
PVA /1 % MWCNT	85	0.895	215	225
PVA /3 % MWCNT	80	0.446	212	225
PVA /5 % MWCNT	74	0.296	210	223

According to the experiment performed by Naebe, et al (2007), there is a significant increase in enthalpy of melting and the degree of crystallinity when PVA is reinforced by MWCNT. The experiment was conducted to test the thermal properties of electrospun PVA reinforced with MWCNTs. However, the values decreased with increasing MWCNT percentage due to agglomeration. Table 2.2 shows the results of DSC data for reinforced PVA/MWCNTs composite.

Table 2.2: Results of DSC Data for Reinforced PVA/MWCNTs Composite (Naebe, et al, 2007)

	T_m(℃)	Δ*H* (J/g)	X (%)	Onset
Pure PVA	218.0	44.6	28.8	215
MWCNT/PVA	221.1	53.2	34.3	201

The melting temperature, enthalpy of melting shows better improvement after reinforcement of MWCNT compared to pure PVA. When the melting temperature increased, more energy is needed to break the bond between PVA composites. Hence, the enthalpy of melting will increase as well. This finding indicates a strong degree of bonding between PVA and MWCNT which effectively prevent the melting process of polymer at its bulk melting temperature (Dassios and Galiotis, 2012). Higher percentage of X (crystallinity) indicated higher degree of crystallinity the composites are.

2.4 Cuttlebone as an Addictive

Bone is a hierarchical structure which consist of mainly hydroxyapatite (HAp) and type I collagen. A typical bone mainly consists of 70% of HAp, 25% of collagen while the rest of the materials is non-collagenous protein and water. Cuttlefish bone is also known as cuttlebone and it possess hard and porous internal structure.

A typical cuttlebone consists of two parts which is dorsal shield and internal lamellar region. The dorsal shield is a hard and dense structure while lamellar matrix has an extreme porosity up to 90%. Lamellar matrix consists of aragonite which is a crystallised form of calcium carbonate ($CaCO_3$) enclosed in a layer of organic material consist of β-chitin.

Due to its exceptional mechanical properties, cuttlebone is useful in developing bone tissue scaffolding. A digital photograph and SEM of the bone are portrayed in Figure 2.16. Based on the experiment performed by Henggu, Ibrahim and Suptijah (2019), the chemical composition of cuttlebone is shown in Table 2.3.

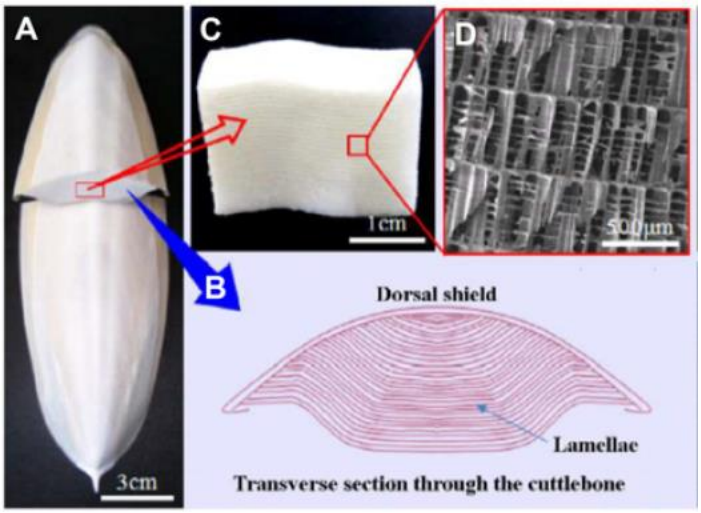

Figure 2.16: (A) Digital Photograph of a Dorsal-View Cuttlebone Cut through the Cross-Section, (B) Schematic Transverse Section through the Cuttlebone, (C) Digital Photograph of A Block Cut from Lamellar Part of the Bone, (D) SEM of the Bone (Momeni, 2013)

Table 2.3: Chemical Composition of Cuttlebone (Henggu, Ibrahim and Suptijah 2019)

Composition	**Parameters (%)**
Moisture	3.54±0.11
Ash	89.61±0.26
Lipid	0.32±0.19
Protein	4.78±0.23
Carbohydrate	5.29±0.02

2.4.1 Calcination of Cuttlebone

According to Henggu, Ibrahim and Suptijah (2019), element apatite lattice can undergo changes when there is exchange of cationic and anionic during the synthesis process. The amorphous and crystallinity of an element depends on the events exchange, ion release and insertion of elements. Figure 2.17 shows the relationship between calcination temperature and the crystallinity of cuttlebone.

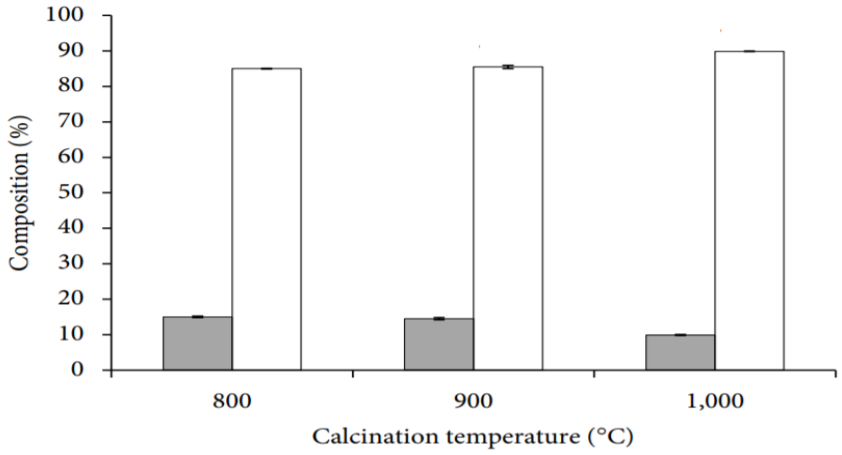

Figure 2.17: Percentage of Apatite Mineral Phase, Amorphous (Grey) and Crystalline (White) (Henggu, Ibrahim and Suptijah 2019)

The crystallinity of a compound is associated with the mechanical strength. As the crystallinity of the material is higher, the mechanical strength is better. When the calcination temperature increases, the percentage of crystallinity phase increases while the amorphous phase decreases. The formation of amorphous is due to the presence of impurities which tends to alter the structure of apatite.

Cuttlebone contains inorganic element in the form of calcium carbonate ($CaCO_3$). $CaCO_3$ is used as a source of calcium oxide (CaO) for the synthesis of HAp. According to Henggu, Ibrahim and Suptijah (2019), the composition of organic matter contains 20 %- 30% and 70% - 80% of inorganic matter. At different calcination temperature, the decomposition process of $CaCO_3$ become CaO due to the changes in absorption region and the transmission intensity. The transmission absorption resulted from calcination at different temperature can be identified through FTIR and it is shown in Figure 2.18.

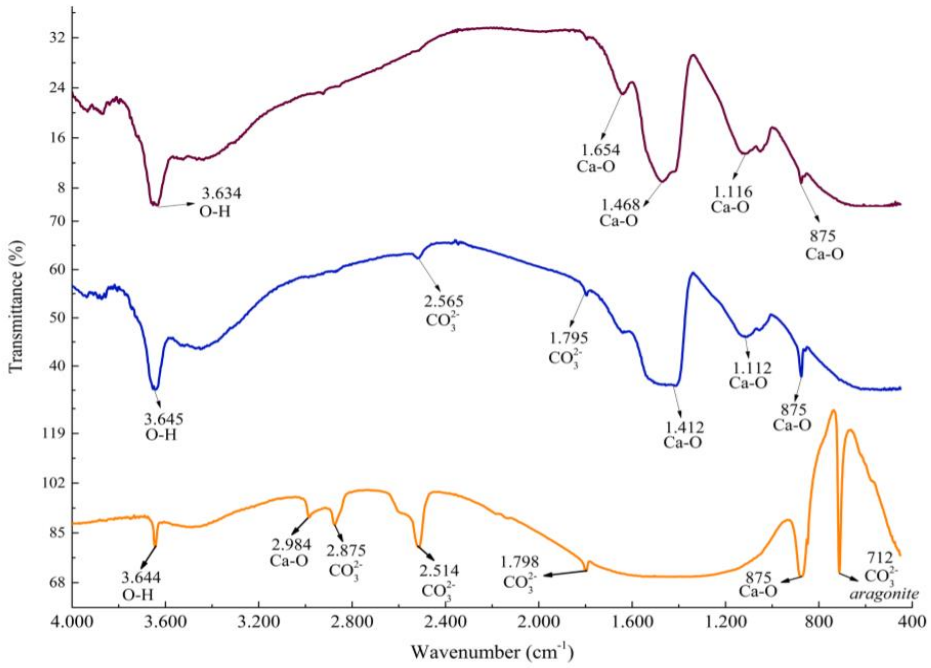

Figure 2.18: FTIR Spectrum of Cuttlebone at Different Calcination Temperature (Henggu, Ibrahim and Suptijah, 2019)

As the calcination temperature increase, more $CaCO_3$ will be decomposed into CaO. The transmission of $CaCO_3$ to CaO is affected by calcination temperature. The process changed in the transmission and led to widening wave, interfering that the elements of $CaCO_3$ contained in the cuttlebone has decomposed into CaO.

2.4.2 Hydroxyapatite (HAp)

In order to further improve the biological properties of cuttlebone-derived HAp, synthetic polymer such as PVA is added to it which gives better properties. HAp is a bioceramic which is chemically similar to the mineral component of bones and it can be obtained naturally or artificially. The natural resources to obtain HAp is by thermal calcination of animal bones such as fish bone, chicken bone and cuttlebone. Extraction of HAp from natural resources is a good alternative due to the useful ions present in it. Besides, it is a promising alterative to Ca and P precursor for the production of thermally stable HAp.

Hydroxyapatite has excellent properties such as biocompatibility, exceptional mechanical strength and osteoconductivity. Due to its similarity to mammalian hard tissue, HAp has undergone investigation for many decades. 24 wt% of Ca, 10 wt% of P, 22 wt% of proteins and trace number of elements like Na^{+}, Zn^{2+} and Mg^{2+} can be found in a typical bone.

The properties of HAp extracted from natural resources depends on extraction techniques, calcination temperature and nature of bones. The organic matter is removed through a calcination regime and to avoid thermal decomposition of the final product.

Thermal calcination is normally used to isolate HAp from natural resources. Calcination process at certain temperature is used to remove the pathogen and the remaining ash contains the mineral compound of the bone. HAp can be obtained by burning the cuttlebone in air furnace. After the heat treatment, black ash will turn into white powder. According to Venkatesan and Kim (2013), the best conditions for achieving nanoparticles is to undergo calcination at 900 ℃ for 8 hours.

Hydroxyapatite is one of the calcium phosphate (CP) based biomaterials having Ca/P molar ratio in the range of 0.5-2 (Akram, et al., 2013). HAp plays an important role as a biomaterial, many attempts are made to improve the biocompatibility of the material. Result shows that HAp with Ca/P ratio of 1.67 exhibits unique biocompatibility and bioactivity (Akram, et al., 2013).

2.4.3 XRD Test on HAp

According to Venkatesan, et al. (2018), cuttlebone has the highest mechanical hardness of 6.87 GPa and the lowest is 4.75 GPa. Cuttlebone is suitable to produce a highly porous scaffold. When the pore size of a scaffold has a range between 100 to 400 μm, the porosity of the scaffold will be more than 90%. The XRD pattern of cuttlebone derived HAp at different calcination temperature is shown in Figure 2.19.

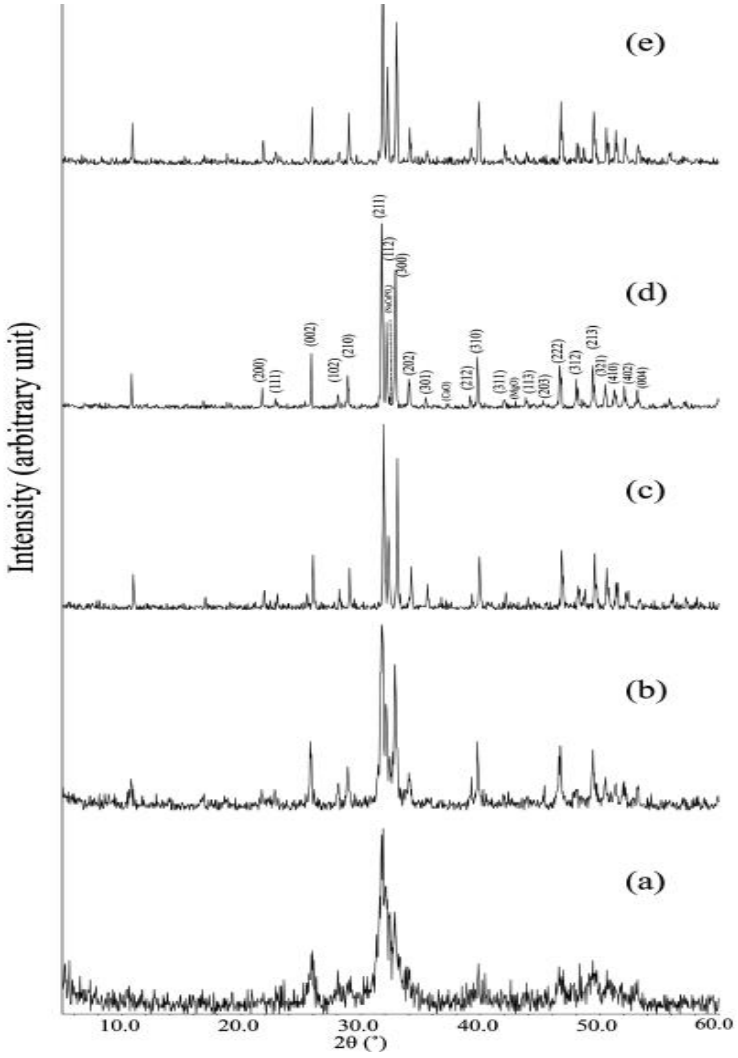

Figure 2.19: XRD Pattern of (a) Bone Ash at Different Temperature; (b) 600 ℃, (c) 700 ℃, (d) 800 ℃ and (e) 1100 ℃ (Bahrololoom, Javidi and Ma, 2009)

As the calcination temperature increased, the peaks became narrower compared to the bone ash with lower calcination temperature. The diffraction pattern of original bone ash is very broad. This is due to the presence of small crystals of hydroxyapatite. The reason which lead to sharpening of the XRD pattern is due to a change of the crystal size of the powder.

The higher the calcination temperature, the larger the crystal size of HAp. In other words, the crystallinity of HAp is higher with higher calcination temperature. From the experiment did by Bahrololoom, Javidi and Ma (2009), the optimum temperature to perform calcination is around 800℃ to 1000℃.

2.5 Bone Scaffolding Reinforced by HAp

Scaffolds play an important role in tissue engineering to direct and support the growth of cells. Ceramic scaffold serves as a template for cell interactions and promote the formation of extracellular matrix in bone. HAp is widely used in bone repair as they have similar chemical and physical properties to the mineral constituents of human bone. HAp is the most thermodynamically stable calcium phosphate ceramic compound and it can form a stable bond with the host tissue. Due to its excellent biocompatibility, bioactivity and osteoconductivity property, HAp is mostly used for the fabrication of inorganic scaffolds.

Scaffold development has attracted much attention as it may overcome the problem of artificial prosthesis transplantation. According to Gervaso, et al. (2011), HAp with finer particle size has more advantage than those with larger particle size. An image of bone scaffold is portrayed in Figure 2.20.

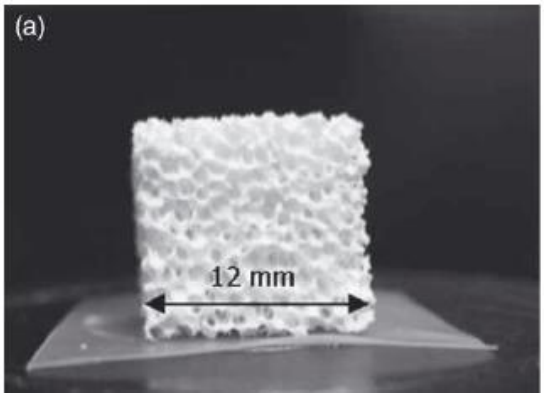

Figure 2.20: Bone Scaffold (Gervaso, et al., 2011)

HAp with nanometer size has superior function due to its particle size and larger surface area to volume ratio. Besides, a finer and porous HAp would have better adsorption of proteins and the crystallinity is similar to biological apatite.

2.5.1 Requirements for an Ideal Scaffold

An ideal scaffold should possess several characteristics to fulfil the requirements of tissue engineering. It must be highly biocompatible which enables the cell growth to attach to the surface. The surface chemistry must be suitable for cell attachment, migration, proliferation and differentiation.

A perfect bone scaffold is important to be osteoconductive in order to allow the bone cells to adhere and grow on its surface and pores as well as to form extracellular matrix. The material should be able to induce strong bond to form osteoconduction and osteoinduction. The scaffold is able to stimulate new bone foundation through biomolecular signalling.

Scaffold with adequate mechanical strength ensure mechanical constancy in load bearing sites. Bone scaffold which is having the same properties with host bone and the implanted scaffold is able to give sufficient mechanical integrity to function from the starting of implantation to the end of the transformation process.

Next, it must be highly porous with an interconnected pore network for cell growth. According to Tripathi and Basu (2011), the ideal pore size of more than 100 μm is allowable for cell penetration and tissue in growth. Table 2.4 shows the pore size distribution for an ideal scaffold in tissue engineering.

Table 2.4: Pore Size Distribution for Ideal Scaffold (Tripathi and Basu, 2011)

Pore Size (μm)	**Biological Function**
<1	Protein interaction, bioactivity
1-20	Cell attachment
100-1000	Cellular growth
>1000	Shape and functionality of implant

Porosity is an important factor to allow movement of cells. The interconnected pores permit movement of cells in multiple directions. Different pore size will have different biological function ranging from protein interaction to functionality of implant.

2.5.2 Advantages of Polymer Composite Scaffolds

Natural, synthetic, semi-synthetic and hybrid materials have been commonly suggested and tested as tissue regeneration scaffolds. Hydroxyapatite is the excellent candidate for bone tissue engineering scaffolding products among synthetic and natural inorganic ceramic products. It plays an extra function in scaffolds, enabling the composite to interact with the bone tissue through a strong bond of carbonate hydroxyapatite layer.

Ceramics are prominent for their excellent compatibility, resistance to corrosion and as well as resistance to compression. However, the disadvantages include fragility, low fracture strength, manufacturing complexity, low mechanical reliability, insufficient resilience, and high density. Polymers are usually flexible and they are lack of mechanical strength, while inorganic materials such as ceramics are too stiff and brittle.

Although these ceramic materials are having osteoconductive characteristics, they are brittle and hard to match the mechanical properties of bone correctly. In addition, ceramic scaffolds were also discovered to be inappropriate for the development of soft tissue. One of the solutions recently being applied in order to overcome the disadvantages is to combine different materials to obtain a composite.

Incorporation of polymer with HAp will improve the mechanical properties due to high stiffness of the inorganic material. Polymer composites shows improved mechanical properties and excellent flexibility. Synthetic polymers are man-made polymers, unlike natural polymers, which can present several benefits as well as greater flexibility and it can be modified into different sizes and forms. The physical-chemical characteristics of such polymers can be readily altered through varying the chemical composition of the macromolecule. The mechanical behaviour and degradation can be appropriately modulated.

Another benefit for this solution is that the polymer phase performs like a carrier for drugs and other biomolecules such as growth factors and this will eventually improve the effectiveness and bioactivity of the scaffolds.

2.6 Polyvinyl Alcohol/ Hydroxyapatite (PVOH /HAp)

Pure materials alone are not able to fulfil all the requirements for biomedical implants. Hence, development of bio-composite materials consists of at least two chemically distinct phases which consist of matrix and nanofiller is used to improve the matrix-filler bonding.

2.6.1 Scanning Electron Microscopy (SEM)

SEM is used to observe the changes on the surface morphology, particle geometry, pore size and porosity of PVOH /HA on different concentrations. Figure 2.21 shows different HA content ranging from 0 wt % to 7.5 wt % in PVOH /HA composite.

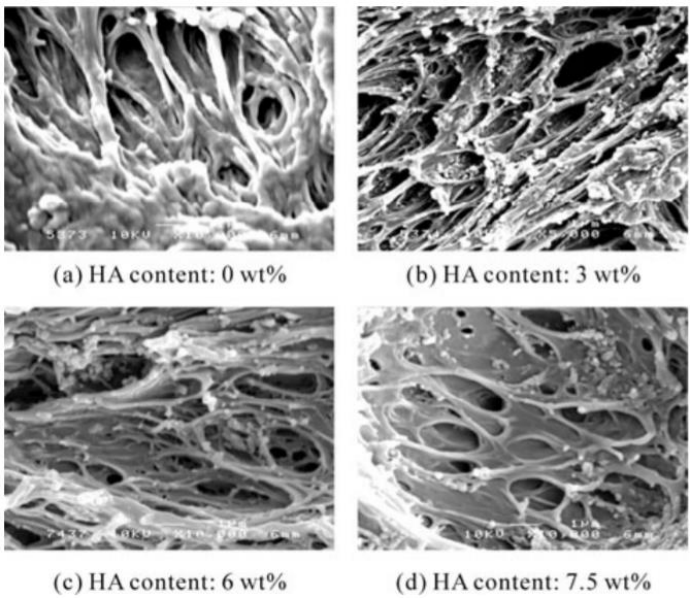

Figure 2.21: SEM Image of HA/PVOH Composite with Various HA Content (Pan and Xiong, 2010)

According to the experiment from Pan and Xiong (2010), 0 % of HA content shows the similar micropore structure of nature cartilage. When the HA content is low, HA particles disperse homogeneously in PVOH matrix. As the HA content increased, large number of HA can be observed. High specific surface area of nano-particles increases the mechanical properties of the composites and eventually led to improvement in interfacial bonding strength. However, the matrix tends to agglomerate as the HA content increased due to its high surface-active energy when minimum HA content is exceeded (Pan and Xiong, 2010).

2.6.2 Fourier Transform Infrared Spectrometry (FTIR)

FTIR spectra is used to analyse the bands characteristics of biocomposite with different HA percentage in PVOH/ HA composite as shown in Figure 2.22.

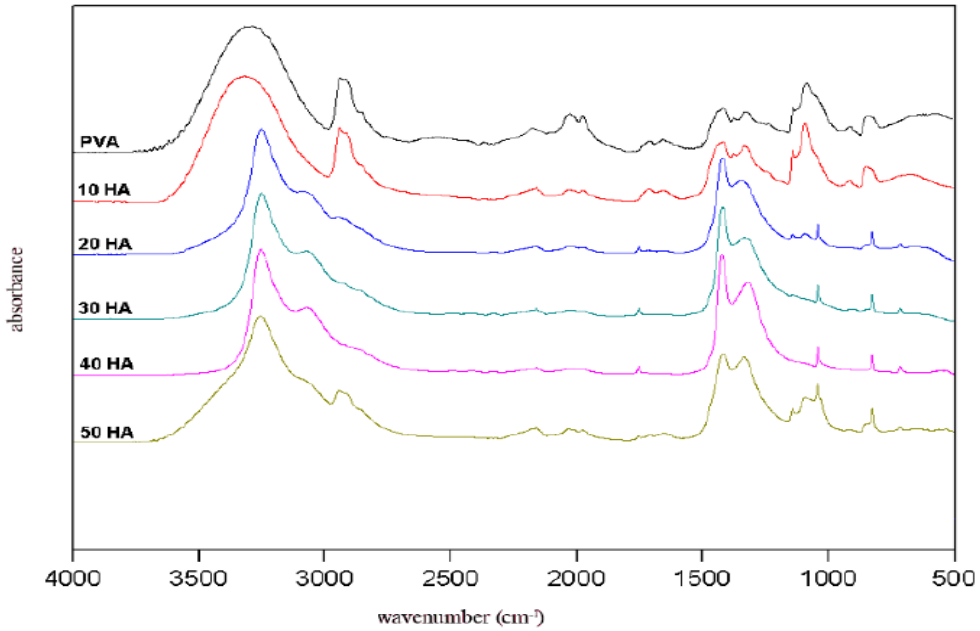

Figure 2.22: FTIR Spectra of Pure PVOH and PVOH/HA Composites (Balgova, et al, 2013)

According to the experiment performed by Balgova, et al. (2013), the intensity of absorbance increased with increasing amount of HA in the composite. The band ranged from 3000 cm^{-1} to 3500 cm^{-1} with maximum band at 3360 cm^{-1} is due to the presence of HA in composite materials. As the amount of HA increased, the PVA spectrum shows a wide and broad band due to the presence of hydroxyl group (-OH) (Balgova, et al, 2013).

CHAPTER 3

METHODOLOGY

3.1 Materials

The materials used in this research were calcined cuttlebones, polyvinyl alcohol (PVOH) and multi-walled carbon nanotubes (MWCNT). The details of each material were listed as follow:

a) Cuttlebone

Raw cuttlebones of 1 kg were obtained from a seafood wholesaler located at Kedah. The cuttlebones were readily to be calcined since they were in a clean and dry condition. Hence, no pre-treatment was required in this research study.

b) Polyvinyl Alcohol (PVOH)

Polyvinyl alcohol (PVA) was obtained from Sekisui Specialty Chemical Co. Ltd. The fully hydrolysed PVA has a viscosity of 4% at 20ºC and hydrolysis of 98.4 mol%.

c) Multi-Walled Carbon Nanotubes (MWCNT)

The type of carbon nanotubes used in this research study was MWCNT. The purity of the MWCNT was more than 90% and they were obtained from Nanjing XFNANO Materials Tech Co. Ltd, China.

3.2 Formulation

A number of calcined cuttlebones varied from 2 phr and 5 phr with constant amount of PVOH at 100 phr were added to different amount of MWCNT in this research study. The manipulated variable was the concentration of MWCNT, which was ranging from 1 phr to 3 phr. Table 3.1 shows the composition of PVOH-MWCNT added with calcined cuttlebone which were used in this research study.

Table 3.1: Composition of PVOH/MWCNT and Calcined Cuttlebone for Preparation of Sample

PVOH (phr)	Calcined Cuttlebone (phr)	MWCNT (phr)
100	2	1
100	2	2
100	2	3
100	5	1
100	5	2
100	5	3

3.3 Sample Preparation

Raw cuttlebones were purchased online. The bones were crushed into powder form using a crusher in order to ease the sample preparation process. The treated cuttlebones were filled into the silica crucible and placed inside the programmable furnace from room temperature to 900℃ for minimum of 4 hours. After calcination process, the cuttlebones were cooled to at least 100℃. The calcined cuttlebones were ready to use in casting process.

The preparation of polyvinyl alcohol composite was solution casting method. One of the sample formulations which involved 2 phr of calcined cuttlebone, 100 phr of PVOH and 1 phr of MWCNT were mixed together. The mixture was stirred at 800 rpm and was heated to 90℃ - 95℃ with hot water bath for 1 hour until the PVOH was completely dissolved. The mixture was poured into the telfon mold and was dried in the oven with temperature of 60℃ to form scaffold. Six samples with different formulation were prepared under the same experimental conditions. The samples were sealed for storage and were kept at the temperature of 25℃ for conditioning purpose.

3.4 Testing

There were several methods used to test the morphology, mechanical, thermal and chemical properties of carbon nanotubes composite.

3.4.1 Tensile Test

The tensile strength of the multi-walled carbon nanotubes (MWCNTs) composite was tested using Instron Universal Testing Machine (Model 4302 Series IX). The test components were Young's modulus, elongation at break and tensile strength. The device used to standardise the sample dimension was ASTM D882. The typical dimension of each samples was 6 cm × 1 cm × 1 cm. The tensile measurement for each different formulation sample were used for six sets of samples.

3.4.2 Scanning Electron Microscope (SEM)

Scanning Electron Microscope (SEM) operated at the electron beam, voltage of 20 kV to 30 kV was used to scan the surface morphology of the sample composite. The type of device used was Hitachi Scanning Electron Microscope (BS 340 TESLA) with a chosen magnification power of 500x to 3000x. A thin layer of gold foil was coated around the sample composite before being scanned by the SEM. The samples were placed facing up in the microscope.

3.4.3 X-ray Diffraction (XRD)

Shimadzu XRD 6000 diffractometer was used to conduct the crystallinity test of the MWCNT composite. The operating condition of XRD was specified to 2θ range of 5° to 70°, current of 30 mA, voltage of 40 kV and scanning length from 0 – 3 cm. The polymer was coated with a thin layer of gold and it was placed on the rotating goniometer which will rotate according to the operating condition. When rotating the goniometer, the change of XRD intensities were recorded. Based on the scanning pattern obtained, the crystallinity and crystallite size of the composite were calculated.

$$Crystallite\ Size, L = \frac{K\lambda}{\beta\cos\theta} \quad (3.1)$$

Where,

L =a measure of the dimension of the particle in the direction perpendicular to the reflecting plane

λ =x-ray wavelength (1.54Å)

β =peak width

θ =angle between the beam and the normal to the reflecting plane

K= constant (taken as 1)

3.4.4 Fourier Transform Infrared Spectroscopy (FTIR)

The chemical properties of MWCNT/PVA with calcined cuttlebone was tested using FTIR. The model of the instrument used was Perkin Elmer Spectrum One. The presence of different functional groups in the MWCNT/PVA with calcined cuttlebone composite were identified by determining the vibration frequency of the different ratio of calcined cuttlebone added with MWCNT. The data transmitted from FTIR was recorded at the end of experiment.

3.4.5 Differential Scanning Calorimetry (DSC)

Differential Scanning Calorimetry (DSC) was conducted by using Perkin Elmer DSC 7 to determine the thermal properties of PVOH/MWCNT/cuttlebone composite. The composite was heated around 25℃ to 240 ℃, with scanning rate of 2℃ min^{-1} for the sample. DSC was used to obtain enthalpy of melting and melting temperature of the composite.

CHAPTER 4

RESULTS AND DISCUSSIONS

4.1 Tensile Strength

Mechanical properties in terms of tensile strength, Young's modulus and elongation at break of the reinforcement of calcined cuttlebone in PVA/MWCNT composite has been studied. Figure 4.1 shows the tensile strength for all the samples. Based on the results from Figure 4.1, the tensile strength increased when amount of MWCNT increased in which the maximum tensile strength is 42.65 MPa for 2 phr calcined cuttlebone and 41.43 MPa for 5 phr calcined cuttlebone. Well mixing of PVA solution into porous MWCNTs network has improved the interfacial bonding between PVA/MWCNT composite and thus increased the mechanical strength.

The tensile strength has decreased from 36.65 MPa to 29.82 MPa from 1 phr to 2 phr of MWCNT at low loading (2 phr) of calcined cuttlebone. The decreasing mechanical properties can be explained by few reasons. MWCNTs have restricted the chain mobility of PVA. Besides, another reason is the complete infiltration of PVA into MWCNTs network (Yee, et al, 2018). Poor dispersion of MWCNTs in PVA, weak interaction between PVA and MWCNTs and bad orientation of MWCNTs and PVA molecular chain are the few reasons which lead to decreasing tensile strength (Lai, et al, 2015). Unlike the previous result, tensile strength of PVA/MWCNT composite has increased from 29.82 MPa to 42.65 MPa when the loading of MWCNT increased from 2 phr to 3 phr.

The tensile strength of PVA/MWCNT composite has increased from 17.69 MPa to 33.26 MPa from 1 phr to 2 phr of MWCNT at high loading (5 phr) of calcined cuttlebone. The tensile strength increased from 33.26 MPa to 41.43 MPa from 2 phr to 3 phr of MWCNT. The result indicates that tensile strength of PVA/MWCNT increased with increasing of MWCNT due to high strength and high aspect ratio of carbon tube (Li,2017). The load of external force can be dispersed along the direction of carbon tube when subjected to external force.

HAp in cuttlebone could enhance the mechanical properties of PVA/MWCNT composite through interfacial interaction between the polymers. The stronger the interfacial interaction, the better the tensile strength. However, when high loading of calcined cuttlebone is added into the PVA/MWCNT composite, the tensile strength has decreased as depicted in Figure 4.1. The tensile strength of PVA/MWCNT composite is higher for 2 phr calcined cuttlebone as compared to 5 phr calcined cuttlebone. The result indicates that HAp served as a reinforced material and could improve the mechanical properties.

A significant drop in tensile strength can be observed when incorporating high loading (5phr) of calcined cuttlebone into PVOH/MWCNT composite compared to low loading (2phr) of calcined cuttlebone. The increasing of particle size and variation of irregular structures of particles causes stress concentration in PVOH/MWCNT composite which lead to low tensile strength.

Besides, the decreasing mechanical properties could be explained upon the addition of calcined cuttlebone into PVOH/MWCNT composite. The formation of agglomerates was due to high viscosity of the matrix and Van der Waals forces among MWCNT (Ferreira, et al., 2017). The ability of composite to resist applied stress was reduced. The degree of uniformity in the composite decreases due to agglomeration of untreated nanoparticles with high surface area. In short, agglomeration weaken the mechanical properties of the composite.

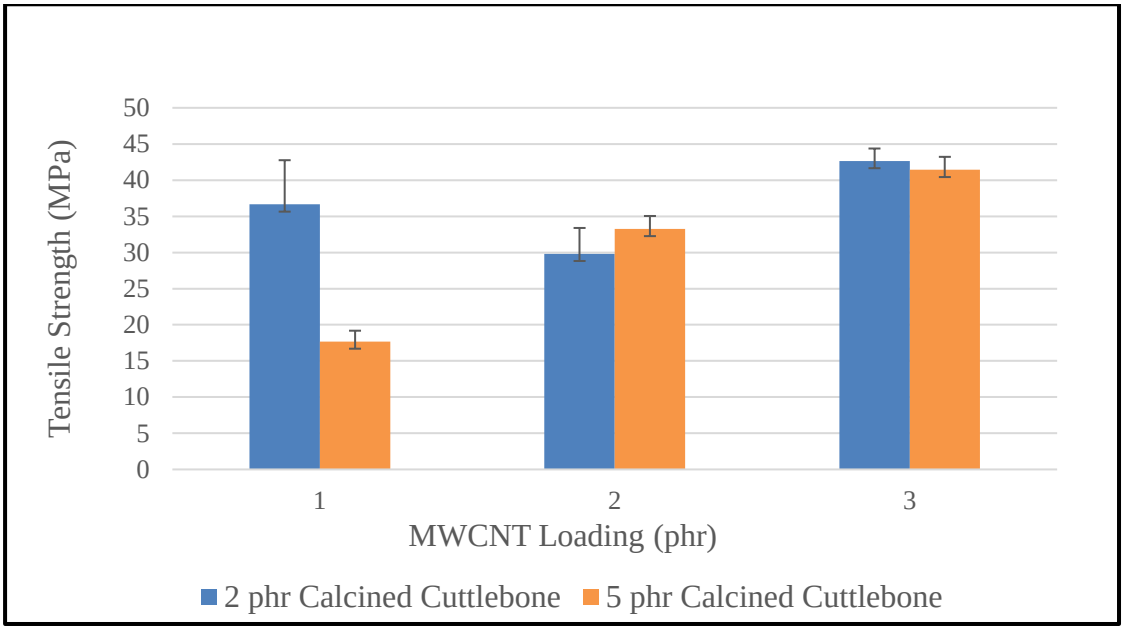

Figure 4.1: Tensile Strength of PVA/MWCNT Composite with Different Loading of Calcined Cuttlebone and MWCNT

4.1.1 Young's Modulus

The Young's modulus of each sample was shown in Figure 4.2. At 2 phr calcined cuttlebone, the Young's modulus has decreased when the amount of MWCNT increased from 1 phr to 2 phr. This phenomenon can be explained by the agglomeration of MWCNT in nanoparticles which causes the tensile strength to decrease. Low Young's modulus indicates that the interaction of MWCNT with PVOH is not well as compared to 3 phr of MWCNTs. When the loading of MWCNT increased to 3 phr, the Young's modulus has increased due to well dispersion of MWCNT in PVOH matrix (Yaser and Toraj, 2013).

At 5 phr calcined cuttlebone, the Young's modulus increased with increasing concentration of MWCNT from 1 phr to 3 phr. Increasing modulus indicates that MWCNT is well dispersed in PVOH matrix. Agglomeration of 1 phr MWCNT in PVA matrix lead to lower Young's modulus as compared to 2 phr and 3 phr of MWCNT. The tear strength increased and less agglomeration occurred in the matrix as the loading of MWCNT increased. The result indicates that appropriate dispersion and interaction of MWCNT in PVA matrix has improved the tearing strength (Yaser and Toraj, 2013).

A significant drop in the Young's modulus graph can be observed when incorporating high loading (5phr) of calcined cuttlebone into PVOH/MWCNT composite compared to low loading (2phr) of calcined cuttlebone. This is mainly due to the dispersion of larger particle in PVA matrix which causes interlocking between particle in PVOH/MWCNT composite.

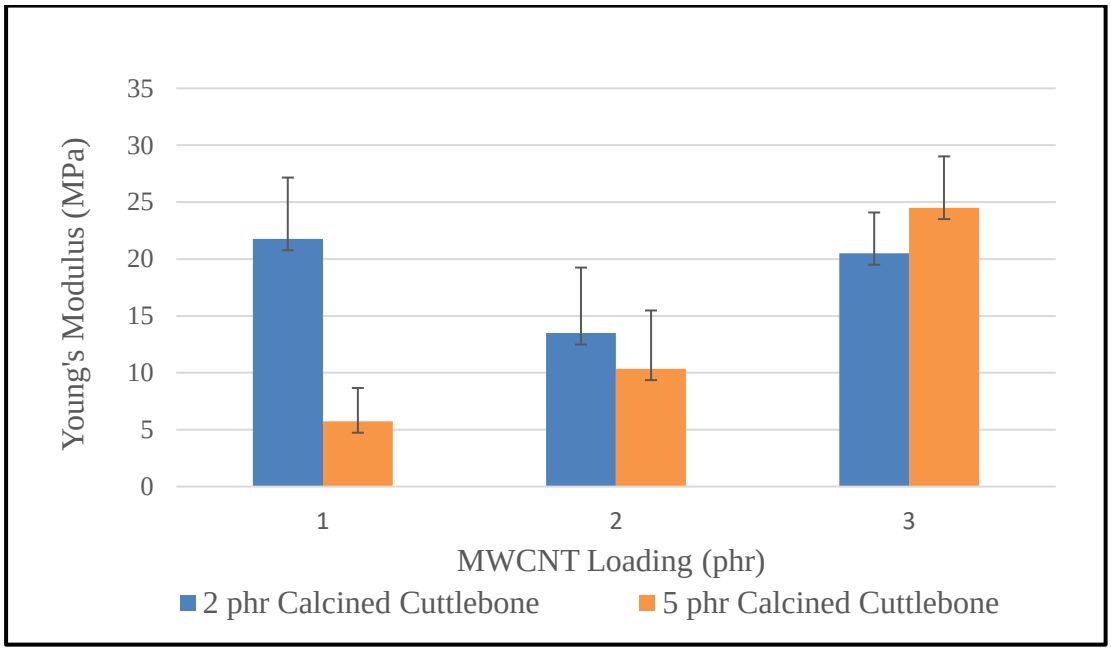

Figure 4.2: Young's Modulus of PVA/MWCNT Composite with Different Loading of Calcined Cuttlebone and MWCNT

4.1.2 Elongation at Break

The results of elongation at break for each sample were shown in Figure 4.3. At 2 phr calcined cuttlebone, the elongation at break increased with increasing MWCNT loading. PVOH with calcined cuttlebone composite is stretcher with higher amount of MWCNT. Small particles of calcined cuttlebone were added into the polymer matrix and leading to improvement of chain sliding between the polymers. The increment of elongation at break indicates that calcined cuttlebone is well mixed and compatible in PVOH/MWCNT composite. Small particles of calcined cuttlebone create lubrication effect with the polymer composite when force is being applied. Strong interfacial binding force between the particles has improved the movement of polymer chain thus increase the elongation at break.

However, at 5 phr calcined cuttlebone, the elongation at break increased at the initial stage and decreased for further incorporation of MWCNT from 2 phr to 3 phr. The elongation at break depends upon the molecular chain's flexibility. The changes on the flexibility is restricted by MWCNT which decreased the elongation of break from 170.47% to 148.33%. This is mainly due to the irregular shape of particles which tend to form stress concentration easily.

In the case of elongation at break, the value is lower at 5 phr calcined cuttlebone as compared to 2 phr calcined cuttlebone at both 1 phr MWCNT and 3 phr MWCNT. However, elongation at break is the highest at 2 phr MWCNT for 5 phr calcined cuttlebone. Large particle of calcined cuttlebone tends to agglomerate which is easily to form stress concentration. Stress concentration is the main reason for low mechanical properties.

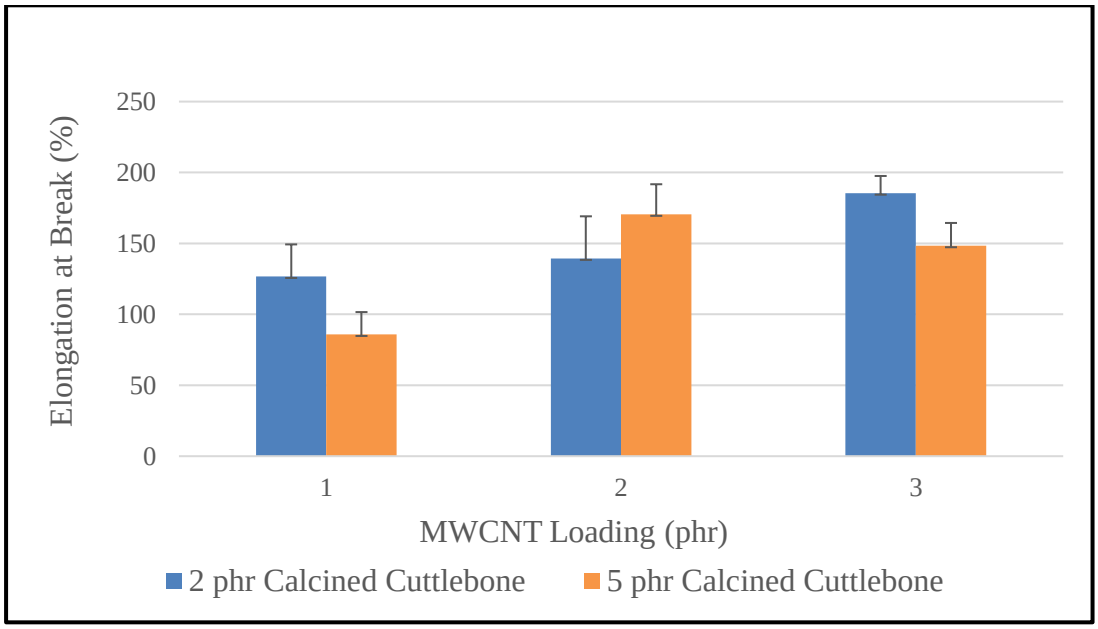

Figure 4.3: Elongation of Break of PVA/MWCNT Composite with Different Loading of Cuttlebone and MWCNT

4.2 Scanning Electron Microscopy (SEM)

The morphology of PVOH/MWCNT with calcined cuttlebone was studied by using SEM micrographs and the results were shown in Figure 4.4 (a)(b)(c) and Figure 4.5 (a)(b)(c). The figure showing SEM images of fractured sample with magnification of x1000. Elongation ability was significantly observed. In general, before adding in the calcined cuttlebone into the polymer matrix, the polymer matrix was having a smooth and continuous surface with no agglomeration occurred. When the amount of MWCNT is low in a polymer matrix, the surface of the nanocomposite is smooth and less rough particles formed on the surface of polymer. The composite has a rough structure as the amount of MWCNT increased in the polymer composite.

At 2 phr calcined cuttlebone, the surface of PVOH/MWCNT composite with calcined cuttlebone became rough and large particle can be observed as the loading of MWCNT increased. At 1 phr of MWCNT, uneven surface and numerous elongated grooves on the composite fiber surface were observed as shown in Figure 4.4(a). Agglomeration were observed in PVOH/MWCNT composite with calcined cuttlebone which would impact the mechanical properties of the polymer matrix.

As the loading of MWCNT increased from 1 phr to 2 phr, more voids or defects appeared between agglomerates and polymer matrix (Lai, et al, 2015). The present of voids in the polymer matrix is the main reason which lead to stress concentration and would cause a sharp declination of tensile strength at 2 phr of MWCNT. However, unlike the previous sample with 1 phr of MWCNT, there were more fibrils with shorter length and the surface was smoother as shown in Figure 4.4(b). Hence, the elongation at break started to increase at 2 phr of MWCNT.

As the loading of MWCNT increased from 2 phr to 3 phr, less fibrils can be observed as compared to low loading of MWCNT as shown in Figure 4.4(c). The result indicates that MWCNT was homogeneously dispersed in polymer matrix resulted in high mechanical strength as discussed in tensile properties.

As shown in Figure 4.4 (a)(b)(c), less agglomeration and a uniform fiber density distribution were observed from the SEM image as compared to Figure 4.5(a)(b)(c), the dispersion of MWCNT was poor in the matrix where many clumps and agglomerate as well as the presence of discontinuities at the boundaries between mixing zone containing different concentrations of dispersed nanofibers were observed.

As the loading of calcined cuttlebone increased from 2 phr to 5 phr, more agglomerates and voids were formed on the surface of polymer matrix. This was mainly due to poor intermolecular chain bond between PVA and causes the polymer matrix to tear into various fibrils as shown in Figure 4.5(a). In addition, the formation of agglomeration on the surface of polymer specifies a higher interaction between the calcined cuttlebone and MWCNT.

As the amount of MWCNT increased to 2 phr, stretches and fiber grooves were obvious in SEM micrograph as shown in Figure 4.5(b). Less agglomerates were observed as compared to 1 phr MWCNT. The result indicates that the polymer matrix was good in terms of its ductility which the film resists to deform and lead to good elongation at break as discussed at tensile properties.

As the amount of MWCNT increased to 3 phr, more fibrils were presented in the SEM micrograph as shown in Figure 4.5(c). The fibrils are short and this may due to the agglomerated particles lower down the intermolecular bonding. Agglomeration which causes lower intermolecular bonding could lead to low tensile strength and elongation at break as compared to low amount of calcined cuttlebone (2 phr).

Voids were spotted in the polymer matrix. Pores in the scaffold were the voids that left after evaporation of water in solvent-rich region during drying process. Poor interactions between MWCNT and calcined cuttlebone added to PVOH when the amount of calcined cuttlebone increased. The agglomeration with voids exists on the composite fracture surface due to poor interactions between MWCNT and the calcined cuttlebone when the amount of calcined cuttlebone increased.

From the results as shown in Figure 4.4(a)(b)(c) and 4.5 (a)(b)(c), MWCNT tends to agglomerate as the amount increased. The occurrence of agglomeration is due to Van Der Waal force has taken place in between the particles and the shape of aggregation is usually in bundle style. Agglomeration weaken the mechanical properties of a polymer composite. Bad dispersibility of MWCNT in a polymer composite is one of the significant reasons for low mechanical strength of PVOH/MWCNT composite as discussed in mechanical properties.

When the HAp content is low, HAp particles disperse homogeneously in PVOH matrix. As the content of HAp increased, large number of HAp can be observed. High specific surface area of nano-particles increased the mechanical properties of the composites and eventually lead to improvement in interfacial bonding strength. However, the matrix will tend to agglomerate as the HAp content increased due to its high surface-active energy when minimum HAp content is exceeded.

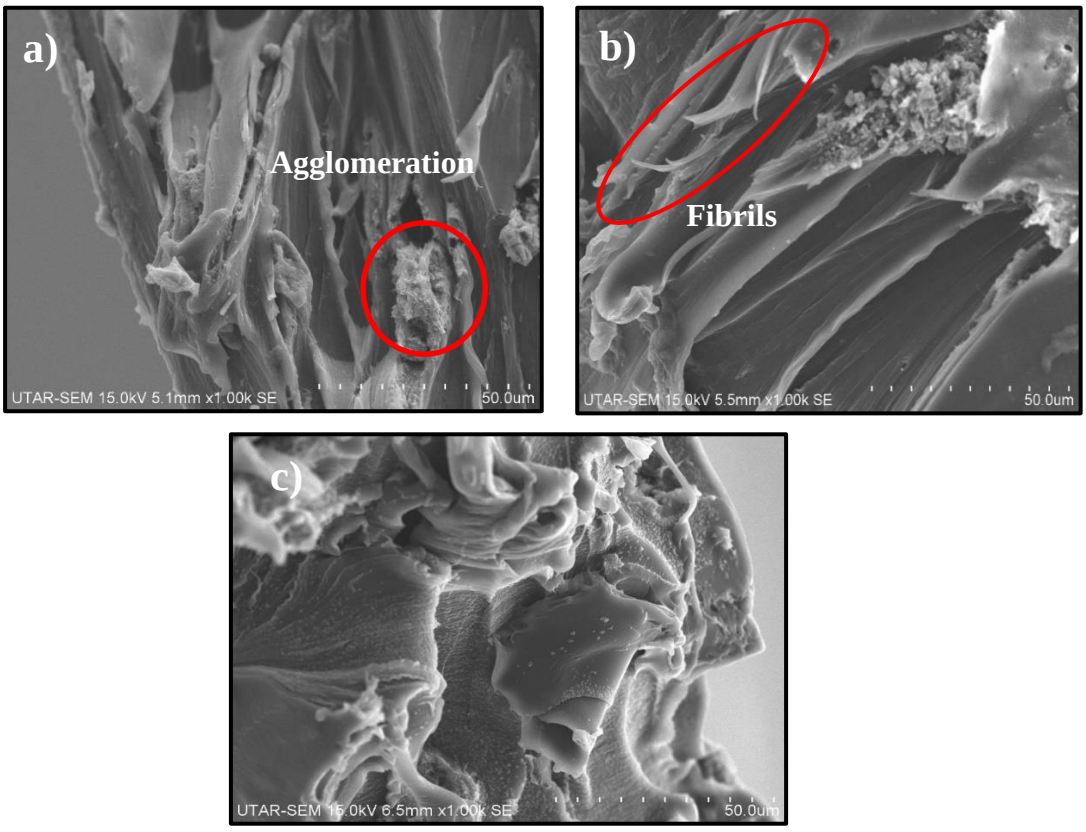

Figure 4.4: Surface Morphology of PVOH/MWCNT Composite at 2 phr of Calcined Cuttlebone added with Different Loading of MWCNT (a) 1 phr MWCNT (b) 2 phr MWCNT (c) 3 phr MWCNT

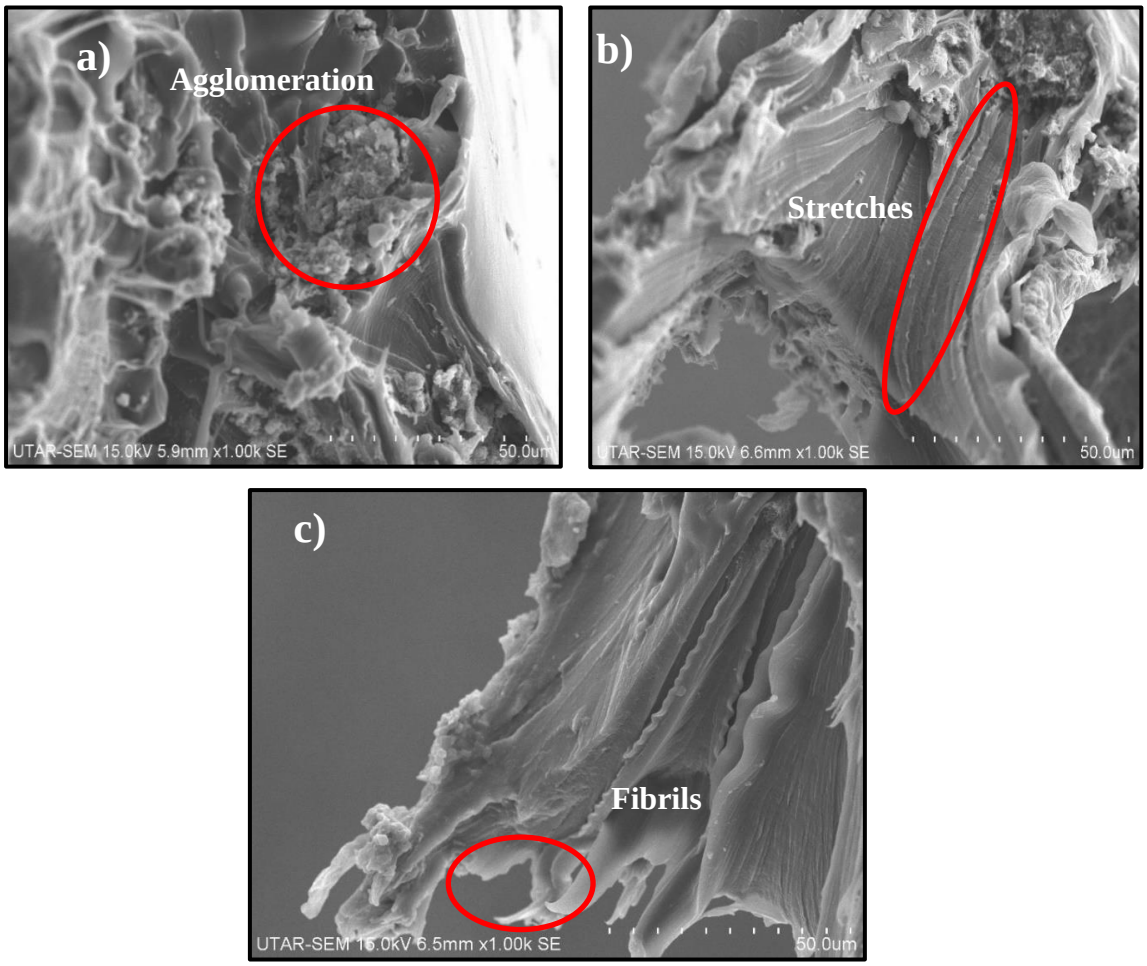

Figure 4.5: Surface Morphology of PVOH/MWCNT Composite at 5 phr of Calcined Cuttlebone added with Different Loading of MWCNT (a) 1 phr MWCNT (b) 2 phr MWCNT (c) 3 phr MWCNT

4.3 X-ray Diffraction (XRD)

In X-ray diffraction analysis, peak position and peak width are the main observations to be analyzed. Several parameters such as crystallinity, crystal size and d-spacing were studied. Range of 3^o to 40^o was used to study the deflection peak for different loading of MWCNT and calcined cuttlebone. Figure 4.6 and 4.7 shows the XRD pattern for all the samples at 2 phr calcined cuttlebone and 5 phr calcined cuttlebone respectively.

4.3.1 Crystallinity of Composite

At both 2 phr and 5 phr calcined cuttlebone, peaks were observed at the range of 19^o-21^o. The peak with intensity appears at $2\theta = 19.6°$ which represents (101) crystal plane (Hajeeassa, et al., 2018). Another peak was observed at 22.9° of the "semi-crystalline" PVA (Diouri and Baitoul, 2013). The diffraction occurred due to "intermolecular interference" between PVA polymer chains. As the intensity of diffraction increased, the number of PVA chains packing increased as well. The peak of calcined cuttlebone can be observed around 31.77°.

As the loading of MWCNT increased from 1 phr to 2 phr, more sharp and narrow peaks were observed. Moreover, a broad peak around 30.9° with high intensity was observed in Figure 4.6. The peak around 19° disappeared from 2 phr to 3 phr of MWCNT. The result was mainly due to the rupture of crystal structure of calcined cuttlebone. Besides, the peak of calcined cuttlebone has shifted from around 30° to 32° with lower intensity. An increase in broadness and decrease in peak intensity have been observed. Therefore, the crystallinity has the highest value as observed in the crystallinity graph as shown in Figure 4.8. In other words, the broadness of peak decrease with increasing loading of MWCNT. The result indicates that the MWCNT is well dispersed in PVOH matrix and crystalline structure was induced. Crystalline structure is orderly arranged with uniform intermolecular forces in the crystal lattice.

At 5 phr calcined cuttlebone, more sharp and narrow peaks were observed from 1 phr to 2 phr of MWCNT. High amount of crystallite peak indicates that crystal structure was induced in the sample. Well dispersion of MWCNT in PVOH matrix can be one of the reasons which causes strong crystallite peak. Moreover, a sharp peak around 27° was observed at 2 phr MWCNT and the peak has disappeared at 3 phr MWCNT. This is mainly due to the rupture of crystal structure of calcined cuttlebone. The sample's peak broadness increased as the loading of MWCNT increased further from 2 phr to 3 phr. Figure 4.7 shows that broad peaks instead of sharp and narrow peaks were observed. Peak broadening effect in the samples were due to crystal defect caused by non-homogenous interaction between the particles in the polymer matrix. More defects were presented in the crystal structure. One of the reasons which contributes to broadening effect is the disturbance of ordered structured arrangement of polymer chain.

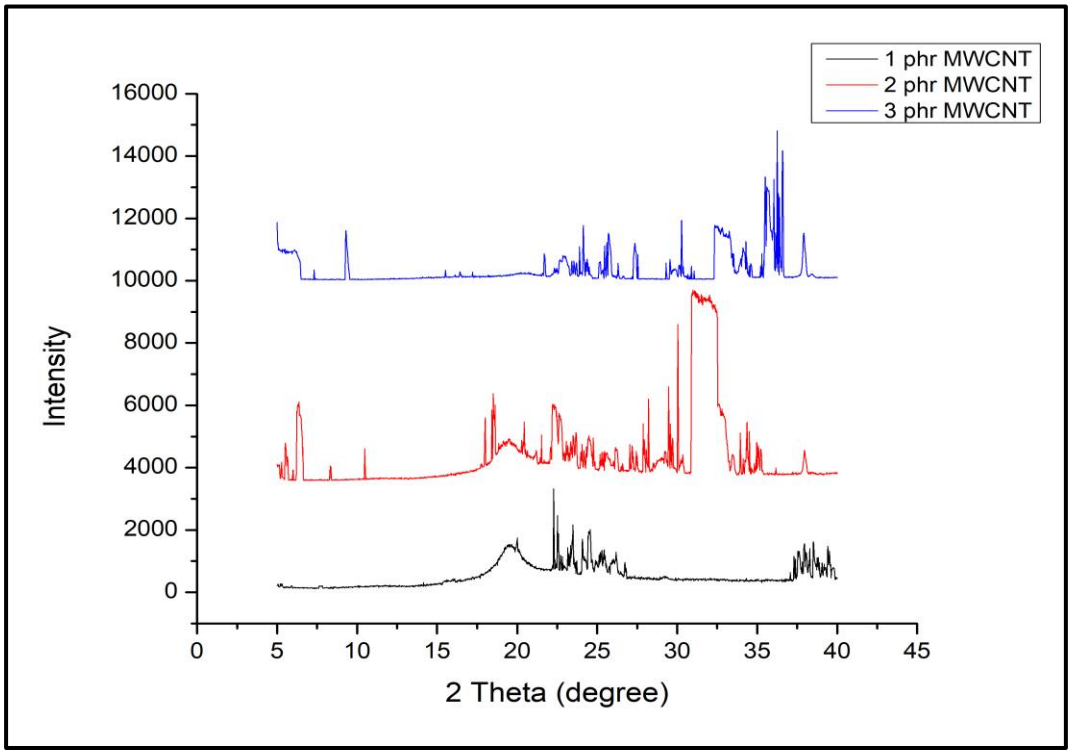

Figure 4.6: XRD Pattern of PVA with Different Loading of MWCNT at 2 phr Calcined Cuttlebone

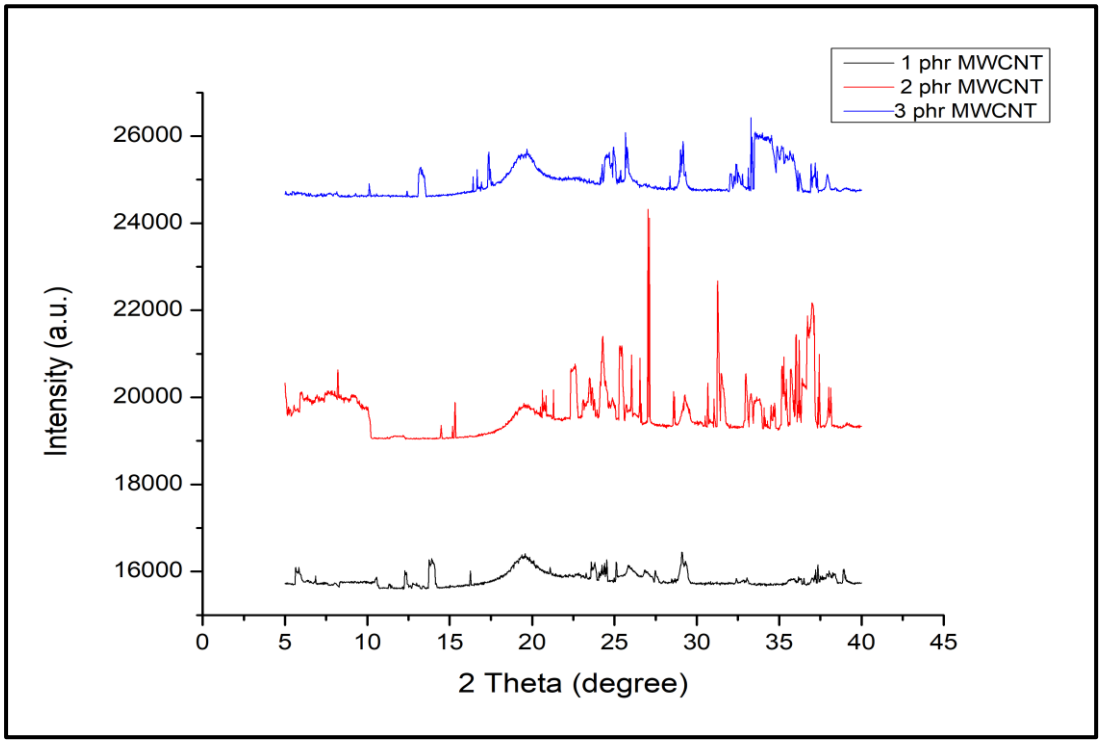

Figure 4.7: XRD Pattern of PVA with Different Loading of MWCNT at 5 phr Calcined Cuttlebone

The increment of crystallinity at 2 phr calcined cuttlebone is due the compactness of matrix as higher loading of MWCNT was added into the polymer composite. At 5 phr calcined cuttlebone, the crystallinity increased from 1 phr to 2 phr of MWCNT then decreased from 2 phr to 3 phr of MWCNT. This is due to crystal defect in polymer composite. As shown in Figure 4.8, the crystallinity of 5 phr calcined cuttlebone is lower than 2 phr calcined cuttlebone. The crystallinity shows the same trend as the XRD graph obtained from Figure 4.6 and 4.7. As the loading of calcined cuttlebone increased from 2 phr to 5 phr, the amount of small crystallite peak decreased. The results indicate that crystallinity decreased as higher amount of nanocomposite is being dispersed in PVA composite. Dispersion of larger particle in PVA matrix causes interlocking between particle and reduced the crystallinity of a component. The decrement in crystallinity upon addition of 5 phr of calcined cuttlebone is mainly due to the particle interaction to form agglomeration which lower the elongation at break.

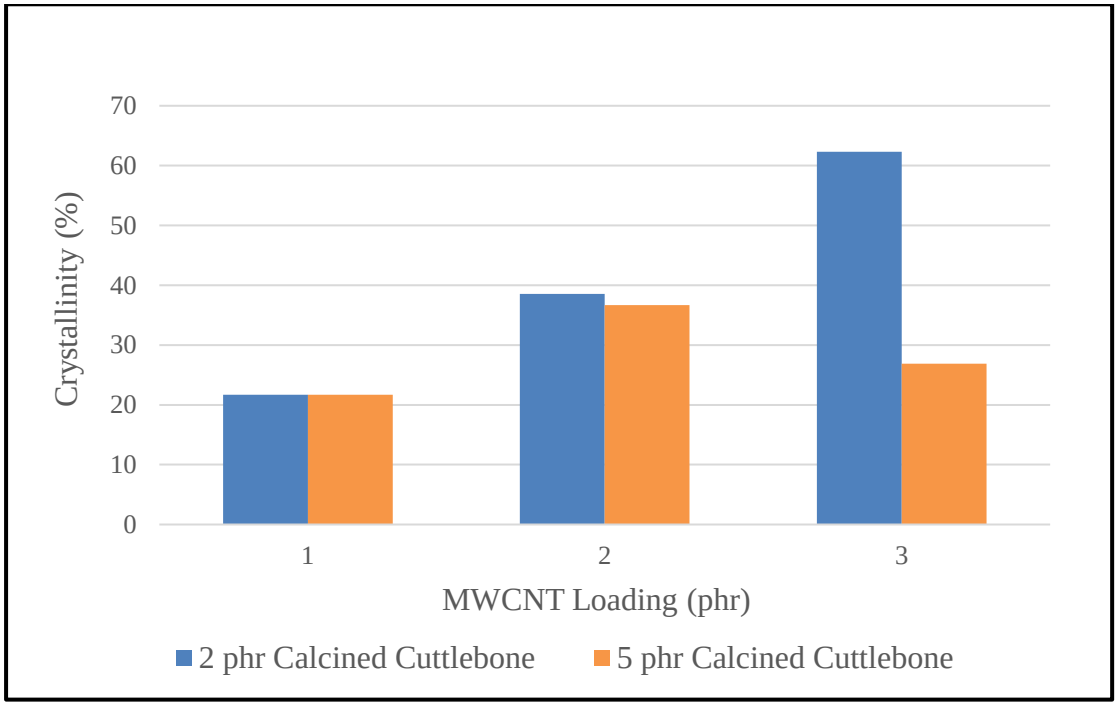

Figure 4.8: Crystallinity of PVA with Different Loading of MWCNT and Calcined Cuttlebone

4.3.2 Crystallite Size of Composite

The crystallite size of the composite was determined by using Scherrer's equation and the result was tabulated in Table 4.1 and 4.2. At 2 phr calcined cuttlebone, the crystallite size decreased from 1 phr to 2 phr of MWCNT in the polymer matrix whereas the crystallite size increased further from 2 phr to 3 phr of MWCNT. According to Scherrer's equation, crystallite size is inversely proportional to peak width. In other words, when the peak width increases, the crystallite size decreases. The results showed the same trend as broadness of peak where the crystallite size decreased from 1 phr MWCNT to 2 phr MWCNT and increased from 2 phr MWCNT to 3 phr MWCNT. As shown in Figure 4.6, the peak broadness increased first then decreased. The results obtained in Table 4.1 has the same trend as Figure 4.6.

At 5 phr calcined cuttlebone, the crystallite size increased when the loading of MWCNT increased from 1 phr to 2 phr in the polymer matrix whereas the crystallite size decreased when the loading of MWCNT increased further from 2 phr to 3 phr. The results showed the same trend as broadness of peak where the peak broadness decreased first then increased as shown in Figure 4.7. The factor which contributes to the changes in crystallite size was intercalation effect.

Intercalation effect captures the polymer inside the interlayer spacing. The intercalation effect shows the characteristics of dispersion of calcined cuttlebone and MWCNT in PVA matrix. The d-spacing is the principle for this characteristic as high d-spacing indicates that intercalation was improved and vice versa. Based on the data tabulated in Table 4.1, d-spacing decreased from 1 phr MWCNT to 3 phr MWCNT whereas as seen in Table 4.2, there is only a slight change in d-spacing where the value decreased from 1 phr MWCNT to 2 phr MWCNT and increased from 2 phr MWCNT to 3 phr MWCNT.

Table 4.1: Crystallite Size and d-Spacing at 2 phr Calcined Cuttlebone

MWCNT Loading (phr)	**Crystallite Size (Å)**	**d-spacing (Å)**
1	761.27	4.44516
2	114.39	3.95866
3	1055.15	3.92433

Table 4.2: Crystallite Size and d-Spacing at 5 phr Calcined Cuttlebone

MWCNT Loading (phr)	**Crystallite Size (Å)**	**d-spacing (Å)**
1	257.28	3.75111
2	315.67	3.57054
3	126.94	3.87035

4.4 Fourier Transform Infrared Spectroscopy (FTIR)

Besides mechanical and physical properties, interaction of bonding between PVOH, MWCNT and calcined cuttlebone was studied. Figure 4.9 shows the FTIR spectrum at 2 phr calcined cuttlebone whereas Figure 4.10 shows the FTIR spectrum at 5 phr calcined cuttlebone. The FTIR spectra of PVOH/MWCNT composite and calcined cuttlebone presented in Figure 4.9 was the evidences of the formation for nanocomposite. The pattern of FTIR spectrum was consistent and the peak was obvious.

As shown in Figure 4.9, broad peak was observed at the range of 3254 cm^{-1} to 3277 cm^{-1} indicating the presence of hydrogen-bonded hydroxyl group of PVA or O-H in COOH groups and absorbed water (Malikov, et al.,2014). The occurrence of stretching mode in region 2917 cm^{-1} to 2927 cm^{-1} were corresponding to two vibration bands which are asymmetric stretching vibration band of CH_3 as well as asymmetric and symmetric stretching bands of CH_2 (Lai, et al, 2015). These bonds are assigned to C-H stretching mode of the backbone of PVOH. Moreover, stretching mode in region 1079 cm^{-1} to 1088 cm^{-1} indicating the presence of C-O-C groups in PVOH matrix (Diouri and Baitoul, 2013). In addition, the presence of peak at the range of 1656 cm^{-1} to 1679 cm^{-1} was attributed to the C double bond (C=C) stretching vibration in graphitic layers. However, functional MWCNT has extra stronger peaks in their spectra. The peak at 1323 cm^{-1} to 1328 cm^{-1} indicates the presence of O-H bending vibration in COOH groups.

Furthermore, peak located at the range of 1153 cm^{-1} to 1162 cm^{-1} was attributed to C-O stretching which contributed the crystallinity phase of PVOH matrix. Another important absorption peak located at the range of 1412 cm^{-1} to 1419 cm^{-1} and 811cm^{-1} to 834 cm^{-1} which can be used to compare the crystallinity of polymer composite at different loading of MWCNT which were corresponding to CH_2 scissoring and rocking deformation (Diouri and Baitoul, 2013). Besides, the effect of MWCNT on the crystallinity of PVOH can be related to the relative intensity of bands located at 1153 cm^{-1} to 1162 cm^{-1} and 1412 cm^{-1} to1419 cm^{-1} (Diouri and Baitoul, 2013). An increasing of intensity favor a better crystallinity in PVOH/MWCNT composite. All of the above results indicate that MWCNT and calcined cuttlebone were introduced into PVOH matrix.

In Figure 4.10, broad peak was observed at the range of 3252 cm^{-1} to 3262 cm^{-1} and the band was attributed to the stretching vibration of -OH group in PVOH. In addition, the peak at the range of 2912 cm^{-1} to 2920 cm^{-1} were due to symmetric and antisymmetric of CH_2 vibration. Besides, the band at the range of 1080 cm^{-1} to 1083 cm^{-1} was attributed to the stretching of C-O group whereas the band at the range of 1562 cm^{-1} was attributed to the C=C stretching in graphitic layer (Lai, et al, 2015). Stretching of C-O group has proved the esterification process between carboxyl groups of MWCNT and hydroxyl (OH) group of PVOH. Additional bonds located at the range of 835 cm^{-1} to 850 cm^{-1} and 909 cm^{-1} to 913 cm^{-1} proves that meta-disubstitution process had occurred between the benzene rings of MWCNT (Malikov, et al.,2014). Moreover, stretching mode in region 1080 cm^{-1} to 1083 cm^{-1} indicating the presence of C-O-C groups in PVOH matrix. The stretching vibration band at the range of 1391 cm^{-1} to 1418 cm^{-1} was attributed to O-H stretching in COOH group (Malikov, et al.,2014). The pattern of FTIR spectrum at 2 phr MWCNT has a strong and sharp peak at 1391 cm^{-1} whereas the peak was absence in both 1 phr MWCNT and 3 phr MWCNT. The reason may due to well dispersion of MWCNT in PVOH matrix which causes strong wavenumber in the sample.

Broad peak around 3252 cm^{-1} to 3277 cm^{-1} corresponds to hydroxyl group (OH). As the loading of calcined cuttlebone increased from 2 phr to 5 phr, the wavenumber for hydroxyl group has a lower value as compared to low loading of calcined cuttlebone (2phr) based on Figure 4.11. A decrement in wavenumber indicates that the interaction between OH group is bad. However, bad interaction of OH group denotes that the hydrogen bonding is strong. Therefore, high loading (5 phr) of calcined cuttlebone leads to stronger hydrogen bond as the OH bonding between the PVOH/MWCNT matrix with calcined cuttlebone was being disrupted. Besides, at 2 phr calcined cuttlebone, the wavenumber increased from 1 phr to 3 phr of MWCNT. On the contrary, at 5 phr calcined cuttlebone, the wavenumber number increased when the loading of MWCNT increased from 1phr to 2 phr and decreased from 2 phr to 3 phr.

Peak at the range of 2912 cm^{-1} to 2927 cm^{-1} corresponds to stretching of C-H bond between the polymer matrix. Based on Figure 4.12, at 2 phr calcined cuttlebone, the wavenumber increased from 1 phr to 3 phr of MWCNT. According to Kuo (2008), physical properties such as amorphous and crystalline structure is one of the factors which affect the strength of molecular bonding within the particles of a sample and it is not only limited to chemical properties such as the type of bonding within particles.

Besides, an increment in the wavenumber indicates that high crystallinity was induced. The result indicates that the crystallinity has increased. The results were proven in XRD crystallinity test as shown in Figure 4.8. An increment in wavenumber is due to high energy is required to overcome the vibration in a confined structure and causes by high shifting of absorption spectra by high crystallinity structure (Kuo, 2008). However, as the loading of calcined cuttlebone increased from 2 phr to 5 phr, the wavenumber is relatively low as compared to low loading of calcined cuttlebone (2 phr). This was due to the dispersion of larger particle in PVA matrix which causes interlocking between particle and reduced the crystallinity of a component. The result indicates that the crystallinity is lower at high loading (5 phr) of calcined cuttlebone and it was proven in XRD characteristic test.

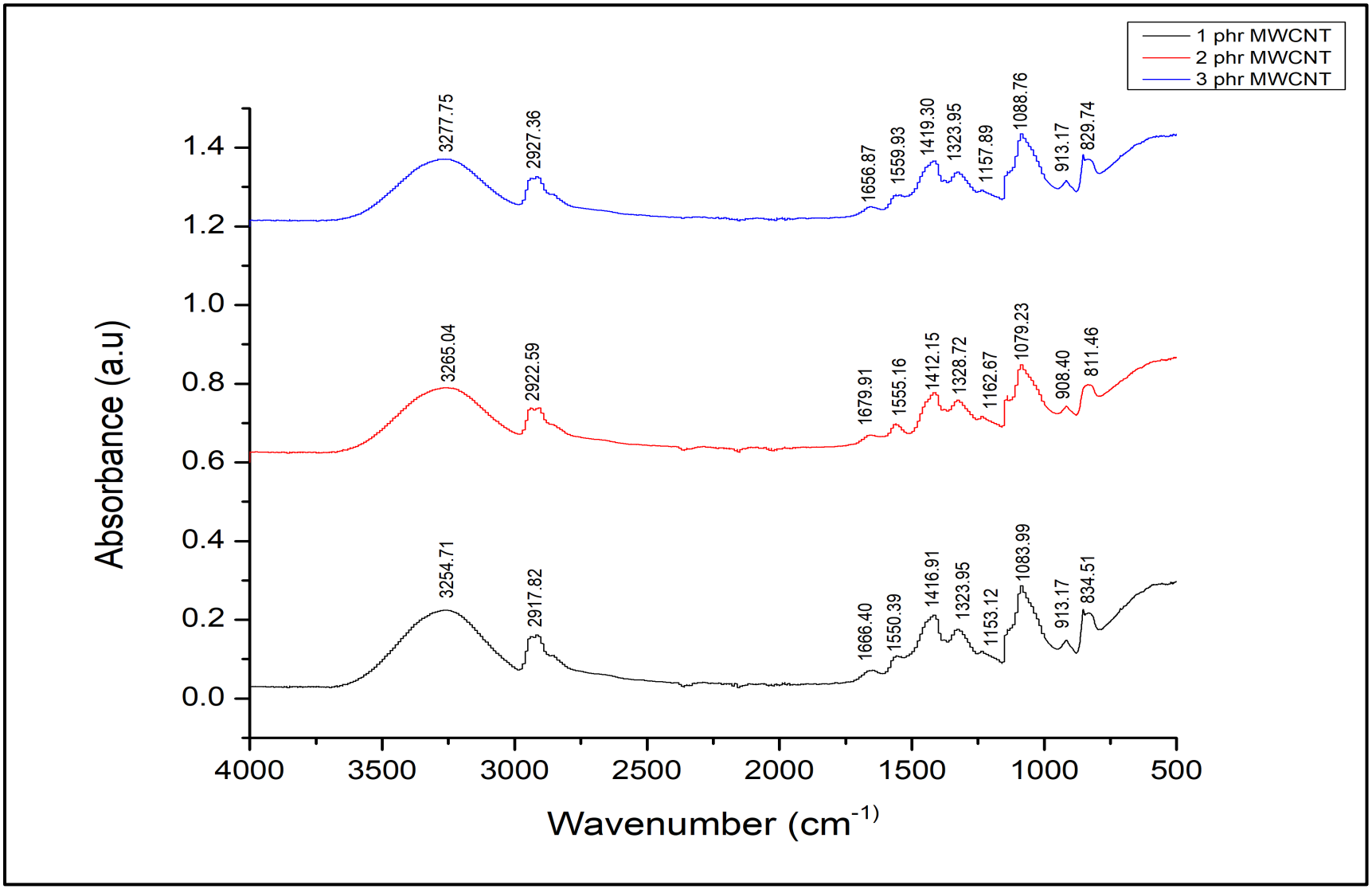

Figure 4.9: FTIR Spectra of PVOH with Different Loading of MWCNT at 2 phr Calcined Cuttlebone

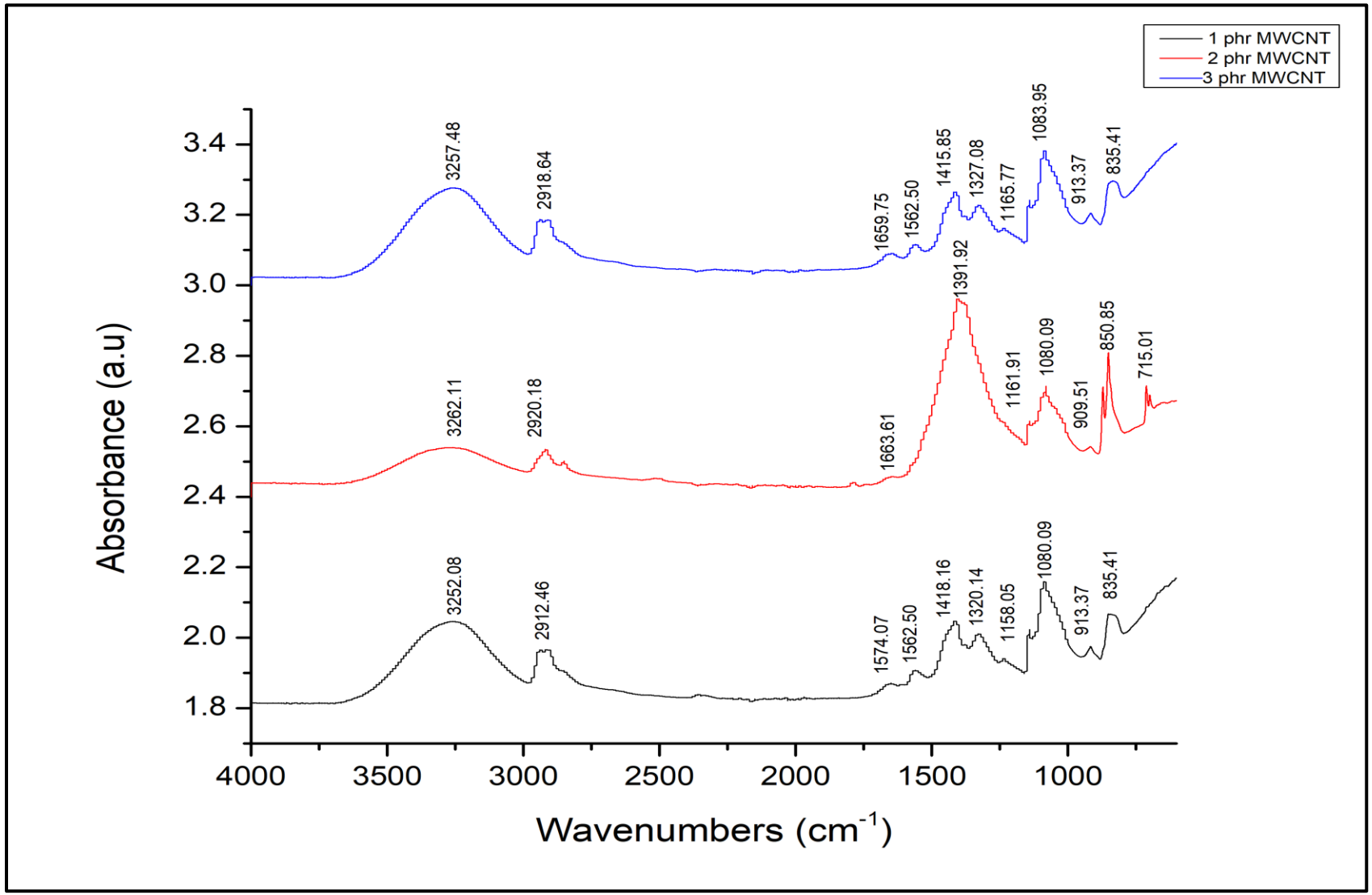

Figure 4.10: FTIR Spectra of PVOH with Different Loading of MWCNT at 5 phr Calcined Cuttlebone

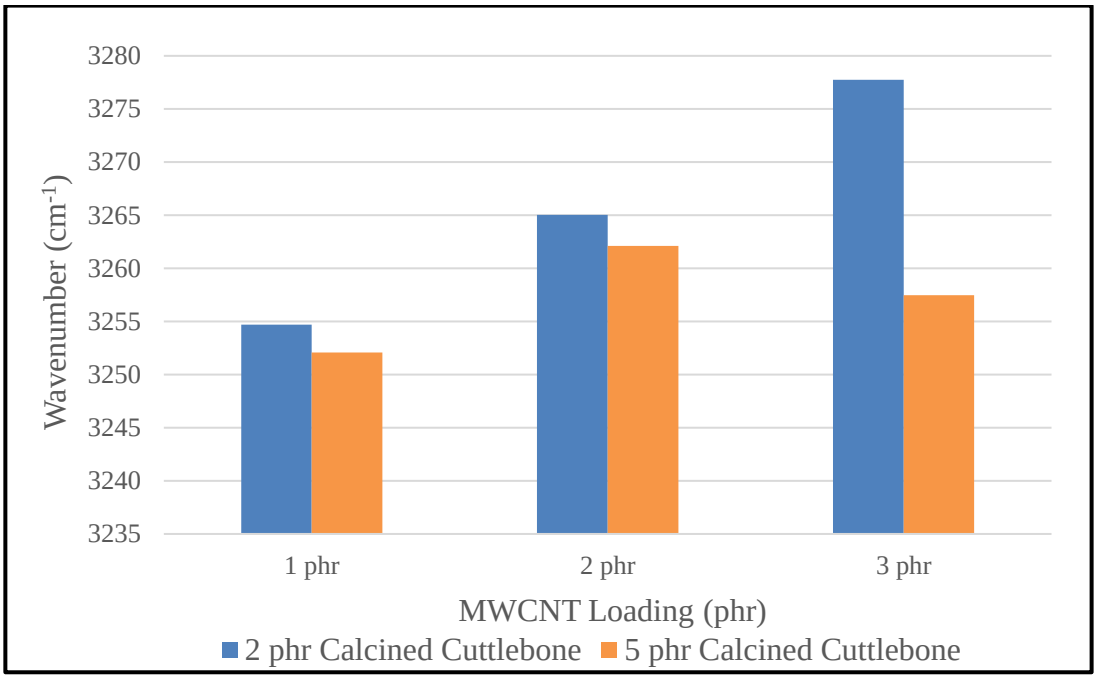

Figure 4.11: Hydroxyl Group of PVOH with Different Loading of MWCNT and Calcined Cuttlebone

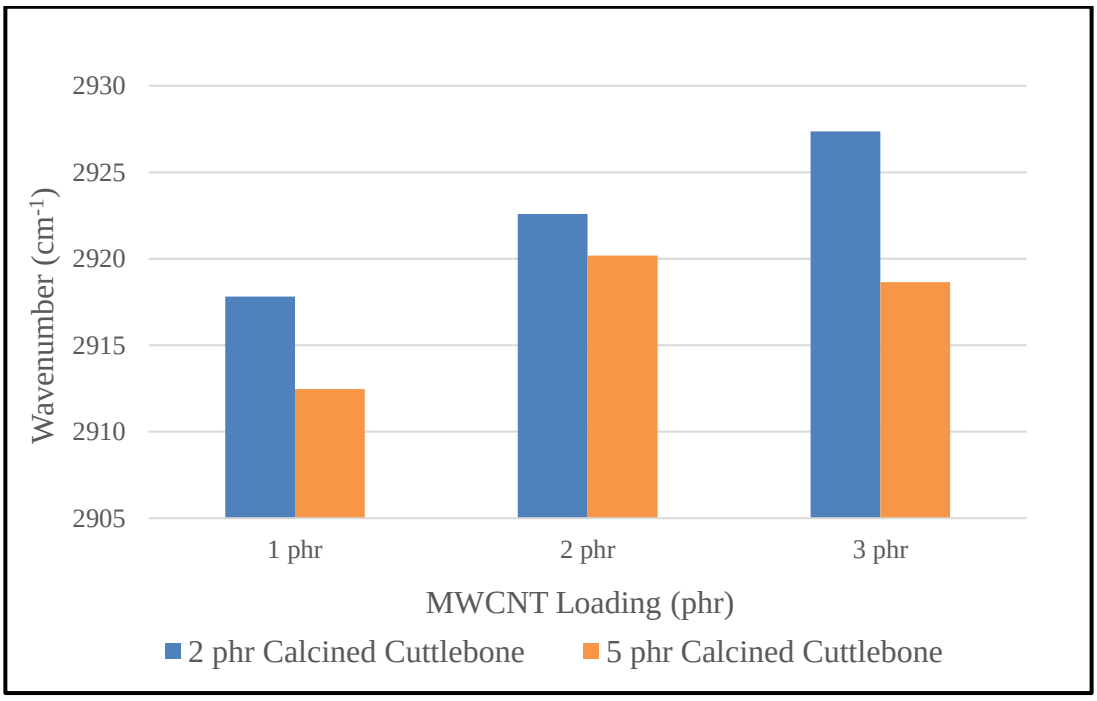

Figure 4.12: C-H Bonds of PVOH with Different Loading of MWCNT and Calcined Cuttlebone

4.5 Differential Scanning Calorimetry (DSC)

DSC test was performed to study the thermal properties of PVA with different loading of MWCNT and calcined cuttlebone by determining the melting temperature and enthalpy of melting of the composite. Figure 4.13 and 4.14 shows the melting temperature curve for all the samples at 2 phr calcined cuttlebone and 5 phr calcined cuttlebone respectively.

4.5.1 Melting Temperature

As shown in Figure 4.13, as the loading of MWCNT increased from 1 phr to 2 phr, the melting temperature increased from 226℃ to 227℃. The melting temperature increased further from 227℃ to 230℃ when the loading of MWCNT increased from 2 phr to 3 phr. In other words, the curve shifted to right from 1 phr to 3 phr of MWCNT. Peak shifting to right indicates that high temperature is needed to melt the composite. The result indicates that upon adding MWCNT in the PVOH matrix causes it to be more rigid due to strong bonding between calcined cuttlebone and PVOH/MWCNT composite.

As shown in Figure 4.14, as the loading of MWCNT increased from 1 phr to 2 phr, the melting temperature increased from 226℃ to 227℃. However, the melting temperature decreased from 232℃ to 230℃ when the loading of MWCNT increased from 2 phr to 3 phr. The curve shifted to right from 1 phr MWCNT to 2 phr MWCNT and shifted to left again from 2 phr MWCNT to 3 phr MWCNT. Decrement in melting temperature is due to agglomeration of MWCNT in PVOH matrix. In addition, another reason which causes decrement in melting temperature is due to the restriction of "chain mobility" in the polymer matrix. The mobility is being restricted by MWCNT in PVA matrix due to strong hydrogen bonding between the oxygen-containing groups of PVOH/MWCNT composite (Lai, et al., 2015). Besides, strong interfacial interaction between calcined cuttlebone and PVOH/MWCNT composite in terms of efficient stress transfer has strengthened the mechanical properties as shown in the previous tensile test which is Figure 4.1.

In general, at high loading (5 phr) of calcined cuttlebone, the melting temperature increased as well. As seen in Figure 4.15, the melting temperature is higher at 5 phr calcined cuttlebone as compared to 2 phr calcined cuttlebone. High melting temperature indicates that the bonding between calcined cuttlebone and PVOH/MWCNT composite is strong.

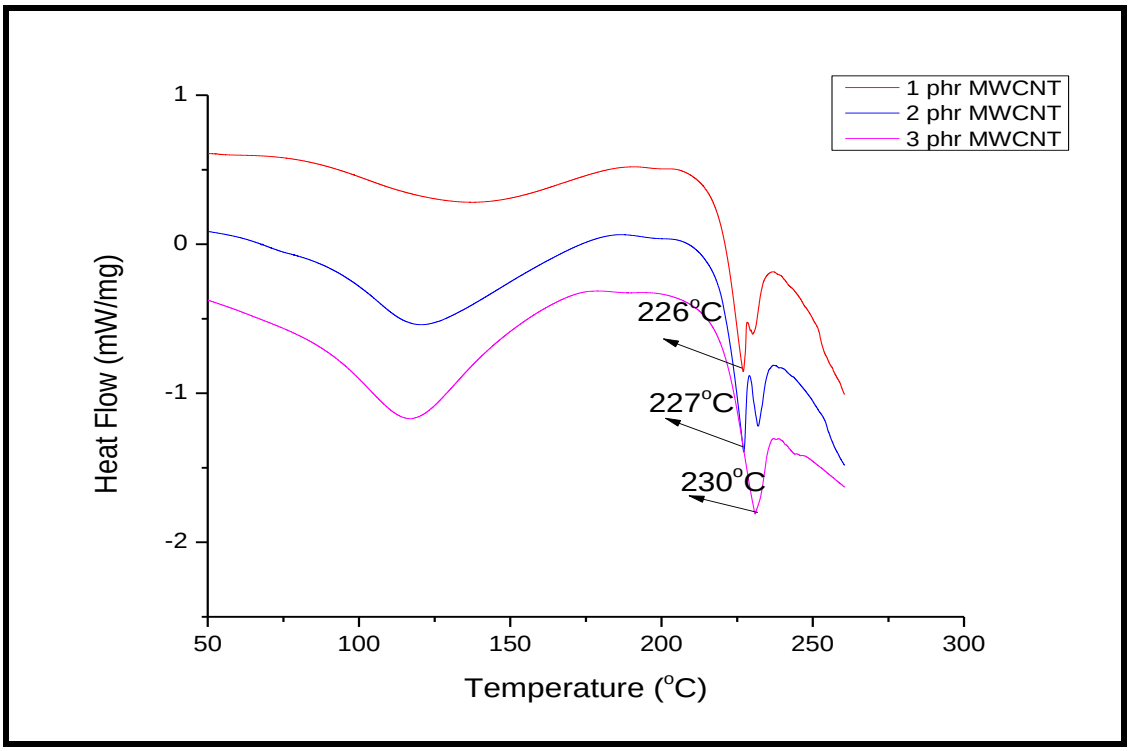

Figure 4.13: DSC Result for PVOH with Different Loading of MWCNT at 2 phr Calcined Cuttlebone

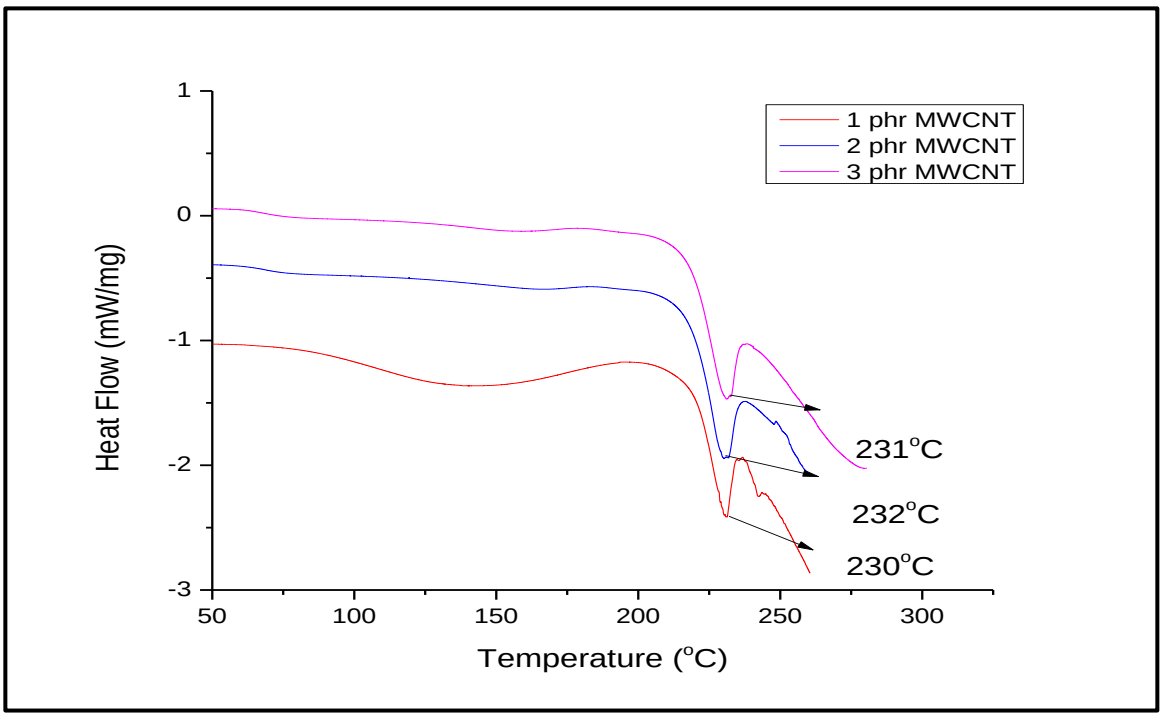

Figure 4.14: DSC Result for PVOH with Different Loading of MWCNT at 5 phr Calcined Cuttlebone

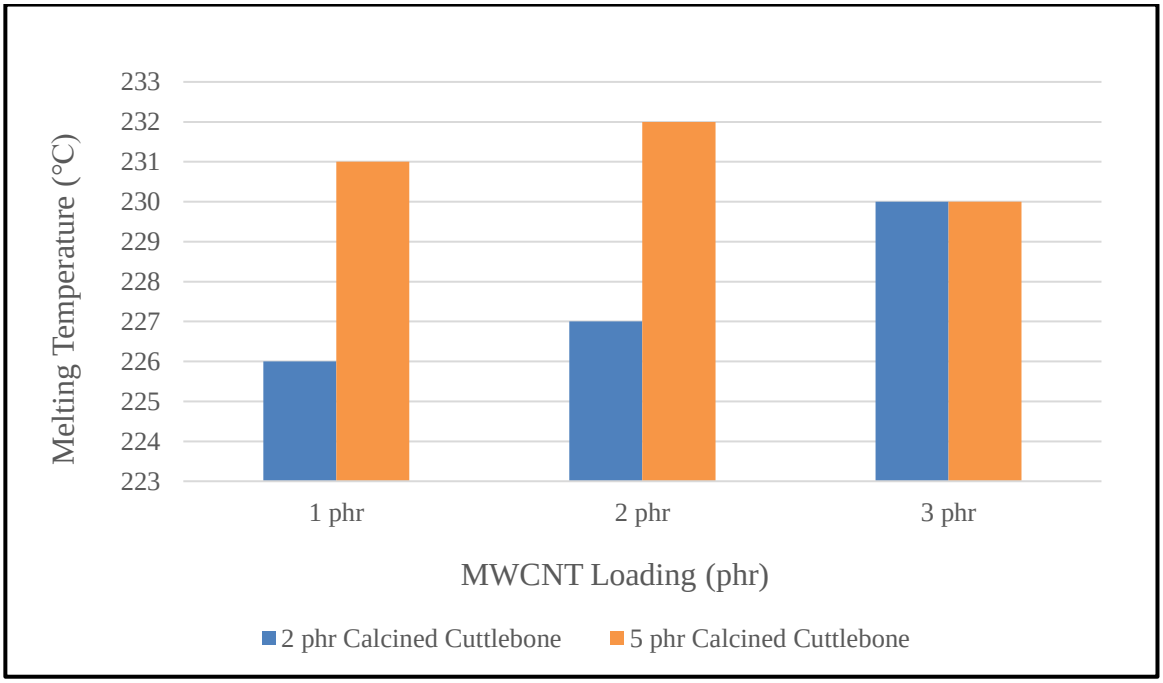

Figure 4.15: Melting Temperature for PVOH with Different Loading of MWCNT and Calcined Cuttlebone

4.5.2 Enthalpy of Melting

The data of enthalpy of melting was recorded and graph was plotted as shown in Figure 4.16. Figure 4.16 shows the comparison of enthalpy of melting for PVOH matrix with different loading of MWCNT at 2 phr and 5 phr calcined cuttlebone.

At 2 phr calcined cuttlebone, the enthalpy of melting decreased from 1 phr MWCNT to 3 phr MWCNT. Decrement of enthalpy of melting indicates the composite is amorphous, thus the elongation at break increased and the results were proven in tensile test which is shown in Figure 4.3. Amorphous structure tends to increase the degree of freedom of the polymer matrix. Hence, less cohesive and disorder composite due to addition of higher loading of MWCNT tends to increase the elongation at break.

At 5 phr calcined cuttlebone, the enthalpy of melting increased from 1 phr MWCNT to 3 phr MWCNT. An increment of enthalpy of melting indicates that the intermolecular interactions between calcined cuttlebone and MWCNT is strong. Hence, higher energy is needed to break the bonding between the composites.

As seen in Figure 4.16, the value of enthalpy of melting at 5 phr calcined cuttlebone is lower as compared to 2 phr calcined cuttlebone at both 1 phr and 2 phr MWCNT. However, the enthalpy of melting for 5 phr calcined cuttlebone is higher as compared to 2 phr calcined cuttlebone at 3 phr MWCNT.

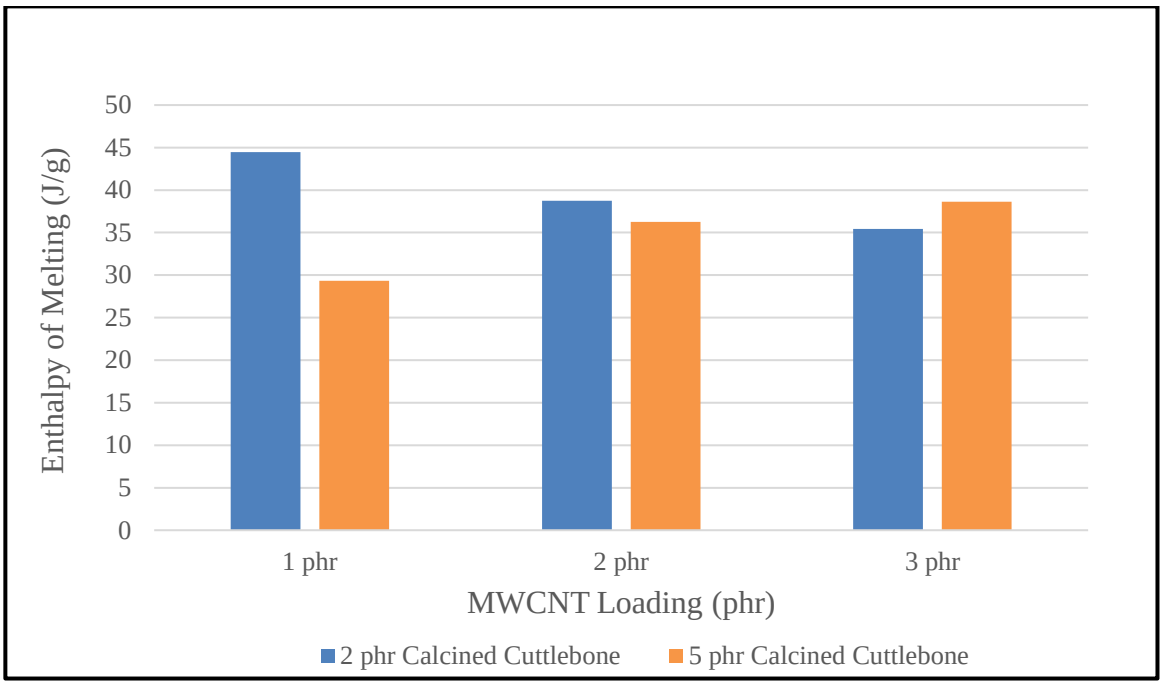

Figure 4.16: Enthalpy of Melting for PVOH with Different Loading of MWCNT and Calcined Cuttlebone

CHAPTER 5

CONCLUSION AND RECOMMENDATIONS

5.1 Conclusion

This study has evaluated the characteristics of polyvinyl alcohol (PVOH) when different loading of calcined cuttlebone and multi-walled carbon nanotube (MWCNT) were incorporated in the polymer matrix. The incorporation of calcined cuttlebone at both 2 phr and 5 phr calcined cuttlebone has significantly increased the tensile strength of PVOV/MWCNT at 3 phr MWCNT. The result indicates that the incorporation of calcined cuttlebone (HAp) served as reinforce phase and improved the mechanical properties of a component. At high loading of calcined cuttlebone (5 phr), the Young's modulus increased with increasing MWCNT. Increasing modulus indicates that MWCNT is well dispersed in PVOH matrix. At low loading (2 phr) of calcined cuttlebone, the elongation at break increased with increment of MWCNT.

Scanning electron microscopy (SEM) results denoted that the surface of PVOH/MWCNT composite with calcined cuttlebone became rough and large particle can be observed as the loading of MWCNT increased. At low loading (2 phr) of calcined cuttlebone, more voids and fibrils appeared between polymer matrix with increasing MWCNT. As the loading of MWCNT increased further, less fibrils can be observed and this indicates that MWCNT was homogeneously dispersed in polymer matrix resulted in high mechanical strength. At high loading (5 phr) of calcined cuttlebone, more agglomerates and voids were formed on the surface of polymer matrix. This was mainly due to poor intermolecular chain bond between PVOH matrix, MWCNT and calcined cuttlebone.

X-ray diffraction (XRD) test depicted that calcined cuttlebone and MWCNT are well dispersed into PVOH matrix. At 2 phr calcined cuttlebone, the broadness of peak decreased with increasing loading of MWCNT. The result indicates that MWCNT is well dispersed in PVOH matrix and crystalline structure was induced. At 5 phr calcined cuttlebone, more sharp

and narrow peaks were observed at the initial stage but the sample's peak broadness increased as the loading of MWCNT increased further. Broadening effect was due to the disturbance of ordered structured arrangement of polymer chain. Besides, the crystallite size decreased and increased at 2 phr calcined cuttlebone whereas at 5 phr calcined cuttlebone, the crystallite size increased and decreased.

Fourier transform infrared spectroscopy (FTIR) test showed that the wavenumber of O-H group increased with increasing loading of MWCNT at 2 phr calcined cuttlebone whereas at 5 phr calcined cuttlebone, the wavenumber number increased first then decreased. A decrement in wavenumber indicates that the hydrogen bonding is strong. For C-H bonds, the wavenumber increased when the loading of MWCNT increased at 2 phr calcined cuttlebone whereas the wavenumber increased then decreased at 5 phr calcined cuttlebone. This was due to interlocking between particle and thus reduced the crystallinity of a component.

Differential scanning calorimetry (DSC) test was performed to determine the melting temperature and enthalpy of melting. At 2 phr calcined cuttlebone, the melting temperature increased with increasing MWCNT loading whereas at 5 phr calcined cuttlebone, the melting temperature increased then decreased. Decrement in melting temperature is due to the restriction of chain mobility between the PVOH/MWCNT, thus leading to strong mechanical properties. At 2 phr calcined cuttlebone, the enthalpy of melting decreased with increasing MWCNT loading whereas at 5 phr calcined cuttlebone, the enthalpy of melting increased with increasing MWCNT loading.

5.2 Recommendations

Studies on the characterization of PVOH added with MWCNT and calcined cuttlebone should be carried out by using thermogravimetric analysis (TGA) in order to study the thermal stabilities in details. Moreover, electron dispersive X-ray (EDX) should be carried out on calcined cuttlebone to analyse the chemical composition and the Ca/P weight ratio of the derived HAp.

REFERENCES

Akram,M.,Ahmen,R.,Shakir,I.,Ibrahim,W.A.W. and Hussain,R.,2013. *Extracting hydroxyapatite and its precursors from natural resources.* Universiti Teknologi Malaysia.

Andrews,R. and Weisenberger,M.C., 2003. Carbon nanotube polymer composites. *Current Opinion in Solid State and Materials Science*,8,pp.31-37.

Andrews,R., Jacques,D., Minot,M. and Rantell,T., 2002. *Macromol. Mater. Eng*,287,pp.295-403.

Aslam,M., Kalyar,M.Z. and Raza,Z.A.,2018. Polyvinyl alcohol: A review of research status and use of polyvinyl alcohol based nanocomposites.*Polymer Engineering and Science.*

Bahrololoom,M.E.,Javidi,M.,Javadpour,S. and Ma,J., 2009. Characterisation of natural hydroxyapatite extracted from bovine cortical bone ash. *Journal of Ceramic Processing Research,* 10(2),pp.129-138.

Balgova,Z.,Palou,M., Wasserbauer,J., Lutisanova,G. and Kozankova,J., 2013. Preparation, characterization and in vitro bioactivity of polyvinyl alcohol hydroxyapatite biphasique membranes.

Cadek,M.M Coleman,J.N., Barron, V., Hediclr,K. and Blau,W.J., 2002. Morphological and mechanical properties of carbon-nanotube-reinforced semicrystalline and amorphous polymer composites. *APPLIED PHYSICS LETTERS*, 81(27),pp. 2-4.

Carreño-Morelli, E., Skripnyuk, V. M., Rabkin, E., Bendersky, L. A., Magrez, A. and Estrin, Y., 2010. Hydrogen storage properties of as-synthesized and severely deformed magnesium – multiwall carbon nanotubes composite.

Dassios,K.G. and Galiotis,C., 2012. Polymer–nanotube interaction in MWCNT/poly(vinyl alcohol) composite mats.*Carbon*, pp. 4291-4301.

Diouri,N. and Baitoul,M., 2013. *Effect of carbon nanotubes dispersion on morphology, internal structure and thermal stability of electrospun poly(vinyl alcohol)/carbon nanotubes nanofibers.* University Sidi Mohammed ben Abdellah: Faculty of Sciences Dhar El Mahraz.

Ekrem,M.,2017. Mechanical Properties of MWCNT Reinforced Polyvinyl Alcohol Nanofiber Mats by Electrospinnig Method. *Journal of Science and Engineering*,4(2), pp.190-200.

Ferreira,F.V.,Franceschi,W.,Menezes,B.R.C.,Brito,F.S.,Lozano,K.,Coutinho ,A.R., Cividanes,L.S. and Thim,G.P., 2017. Dodecylamine functionalization of carbon nanotubes to improve dispersion, thermal and mechanical properties of polyethylene based nanocomposites. *Applied Surface Science*,410,pp.267-277.

Gaaz,T.S.,Sulong,A.B., Akhtar,M.N.,Kadhum,A.A.H., Mohamad,A.B. and Ahmed,A.A., 2015. Properties and Applications of Polyvinyl Alcohol, Halloysite Nanotubes and Their Nanocomposites. *Molecules*,20,pp.22833-22847.

Gervaso,F., Scalera,F., Kunjalukkal,S.P.,Sannino,A. and Licciulli,A., 2011. High-Performance Hydroxyapatite Scaffolds for Bone Tissue Engineering Applications. International Journal of Applied Ceramic Technology,9(3),pp.2-11.

Hajeeassa,S.K, Hussein, M.A, Anwar,Y, Tashkandi,N.Y. and Al-amshany, Z.M., 2018. Nanocomposites Containing Polyvinyl Alcohol And Reinforced Carbon-Based Nanofiller: A Super Effective Biologically Active Material. Original Research Article, 5(1-12).

Hang,N., 2011. *Preparation and Applications of Polyvinyl Alcohol-funtionalized Multiwalled Carbon Nanotubes for Proton Exchange Membrane Fuel Cells*. Degree. WORCESTER POLYTECHNIC INSTITUTE.

Hasan,M., Das,S.K., Islam,J.M.M., Gafur,M.A.,Hoque,E. and Khan.M.A.,2013. Thermal Properties of Carbon Nanotube (CNT) Reinforced Polyvinyl Alcohol (PVA) Composites. *International Letters of Chemistry, Physics and Astronomy*,12,pp.59-66.

Henggu,Ibrahim,B. and Suptijah,F., 2019. Hydroxyapatite of Shell Cuttlefish As Stocks.Biomaterials Scaffolding Bone. *Journal of Fishery Products Processing Indonesia*,22(1),pp.1-13.

Int. J Hydrogen Energy. 35,pp. 5471–5478, doi:10.1016/j.ijhydene.2010.03.047.

Jogi, B.F., Sawant,M., Kulkarni,M. and Brahmankar,P.K., 2012. Dispersion and Performance Properties of Carbon Nanotubes (CNTs) Based Polymer Composites: A Review. *Journal of Encapsulation and Adsorption Sciences*,2, pp.69-78, http://dx.doi.org/10.4236/jeas.2012.24010.

Kaur, T. and Thirugnanam ,A.,2016. Tailoring in vitro biological and mechanical properties of polyvinyl alcohol reinforced with threshold carbon nanotube concentration for improved cellular response. 6(46),pp.39982–39992.

Kaur, T., Thirugnanam. A. and Kar, S., 2016. Microwave-assisted synthesis of porous chitosan–modified montmorillonite–hydroxyapatite composite scaffolds. *International Journal of Biological Macromolecules,* 82, pp. 628-636.

Kuo,S.W.,2008. Hydrogen-bonding in polymer blends. *Journal of Polymer Research,* 15,pp.459-486.

Lai,D., Wei,Y., Zou,L., Xu,Y and Lu,H., 2015. Wet spinning of PVA composite fibers with a large fraction of multi-walled carbon nanotubes. *Progress in Natural Science :Materials International*,25,pp.445-452.

Leszczynska,A. and Pielichowski,K.,2008. APPLICATION OF THERMAL ANALYSIS METHODS FOR CHARACTERIZATION OF POLYMER/MONTMORILLONITE NANOCOMPOSITES. *Journal of Thermal Analysis and Calorimetry*,93(3), pp.677-687.

Li,J.,2017. Multiwalled Carbon Nanotubes Reinforced Polypropylene Composite Material. *Journal of Nanomaterials,*pp.1-5.

Maghfirah,A., Yudianti,R., Fauzi, Sinuhaji,P.,Lektro and Hutabarat,G., 2018. Preparation Of Poly(Vinyl) Alcohol – Multiwalled Carbon Nanotubes Nanocomposite As Conductive And Transparent Film Using Casting Method. *Journal of Physics*,pp.3-6.

Malikov, E.Y., Muradov ,M.B., Akperov, O.H., Eyvazova,G.M., Puskás ,R., Madarász ,D., Nagy ,L., Kukovecz ,Á. Kónya, Z.,2014. Synthesis and characterization of polyvinyl alcohol based multiwalled carbon nanotube nanocomposites. *Physica E*,61,pp.129-134.

Momeni,S., 2013. Cuttlebone: Characterization and Applications Preparative,*Biochemistry & Biotechnology*, 43,pp.696–716.

Naebe,M., Lin,T., Tian., Dai,L. and Wang,X., 2007. Effects of MWNT nanofillers on structures and properties of PVA electrospun nanofibres. *Nanotechnology*, 18, pp.2-9.

Oliveira,A.D. and Beatrice,C.A.G., 2018. Polymer Nanocomposites with Different Types of Nanofiller.

Pan,Y. and Xiong,D., 2010. Preparation and Characterization of Nanohydroxyapatite /polyvinyl Alcohol Gel Composites,25(3),pp.2-5.

Sankar,N.,Reddy,M.N. and Prasad,R.K., 2015. Carbon nanotubes dispersed polymer nanocomposites: mechanical, electrical, thermal properties and surface morphology.*Bull.Mater.Sci*,39(1),pp.47-55.

Sichina,W.J.,2019. Characterization of Polymers Using TGA. PerkinElmer Instruments.

Spitalsky, Z., Tasis, D., Papagelis, K. and Galiotis,C., 2010. Carbon nanotube–polymer composites: Chemistry, processing, mechanical and electrical properties. *Progress in Polymer Science*, 35(3), pp. 357-401.

Spitalsky,Z., Tasis,D.,Papagelis,K. and Galiotis,C., 2010. Carbon Nanotube–Polymer Composites: Chemistry, Processing, Mechanical and Electrical Properties. *Progress in Polymer Science*, 35(3),pp.357-401,doi: 10.1016/j.progpolymsci.2009.09.003

Tontowi, A.E., Perkasa, D.P., Siswomihardjo, W. and Darwis, D., 2018. Effect of Polyvinyl Alcohol (PVA) Blending and Gamma Irradiation on Compressive Strength of FHAp/FGel Composite as Candidate of Scaffold. *International Journal of Engineering and Technology (IJET)*, 8(1), pp. 108-116.

Tontowi,A.E., Perkasa,D.P., Siswomihardjo,W. and Darwis,D.,2016. Effect of Polyvinyl Alcohol (PVA) Blending and Gamma Irradiation on Compressive Strength of FHAp/FGel Composite as Candidate of Scaffold. *International Journal of Engineering and Technology (IJET)*,8(1),pp.1-9.

Tripathi,G. and Basu,B.,2011. A porous hydroxyapatite scaffold for bone tissue engineering: Physico-mechanical and biological evaluations. *Ceramics International*, 38,pp.341-349.

Venkatesan, J., Rekha, P.D., Anil, S., Bhatnagar,I., Sudha, P.N., Dechsakulwatana, C., Kim, S.K. and Shim,M.S., 2018. Hydroxyapatite from Cuttlefish Bone: Isolation, Characterizations, and Applications. *Biotechnology and Bioprocess Engineering*, 23(4), pp. 383-393.

Venkatesan,J. and Kim,S.J., 2013. Hydroxyapatite from Marine Fish Bone, doi: 10.1201/b14723-4.

Venkatesan,J., Rekha,P.D., Anil,S., Bhatnagar,I.,Sudha,P.N., Dechsakulwatana,C., Kim,S.K. and Min,S.S., 2018. Hydroxyapatite from Cuttlefish Bone: Isolation, Characterizationsand Applications. *Biotechnology and Bioprocess Engineering*, 23,pp. 383-393.

Wongon,J., Thumsorn,S. and Srisawat,N.,2016. Poly(vinyl alcohol)/multiwalled carbon nanotubes composite nanofiber. *Energy Procedia*,89,pp.313-317.

Yaser,S. and Toraj,M.,2013. Effects of CNTs Content on Physicochemical and Pervaporation Separation Properties of PVA Membranes. *Separation Science and Technology*,,48,pp.716-727.

Yee,M.J., Mubarak,N.M., Khalid,M.,Abdullah,E.C. and Jagadish,P., 2018. Synthesis of polyvinyl alcohol (PVA) infiltrated MWCNTs buckypaper for strain sensing application.

Yellampalli, S., 2011. Carbon Nanotubes – Polymer Nanocomposites. In: Choudhary, V. and Gupta, A., 2011. *Polymer/Carbon Nanotube Nanocomposites.* Croatia: InTech. Available at: InTech.pp. 2-17.

Yu,M.F., Files,B.S.,Arepali,S. and Ruoff,R.S., 2000. Tensile Loading of Ropes of SingleWall Carbon Nanotubes and their Mechanical Properties. *PHYSICAL REVIEW LETTERS*, 84(24),pp.1-4.

Yu,M.F., Lourie,O., Dyer,M.J., Moloni,K., Kelly.T.F and Ruoff,R.S.,2000. *Strength and Breaking Mechanism of Multiwalled Carbon Nanotubes Under Tensile Load*. Washington University: Department of Physics